Organic self-assembled monolayers for reconstitution of ion channels on single crystal silicon

by

Maryna Ornatska

A thesis submitted to the graduate faculty

in partial fulfillment of the requirements for the degree of

MASTER OF SCIENCE

Major: Materials Science and Engineering

Program of Study Committee:
Vladimir V. Tsukruk (Major Professor)
Thomas D. McGee
Yeon-Kyun Shin

Iowa State University

Ames, IA

2003

Graduate College
Iowa State University

This is to certify that the master's thesis of

Maryna Ornatska

has met the thesis requirements of Iowa State University

Signatures have been redacted for privacy

TABLE OF CONTENTS

ACKNOWLEDGEMENTS

I am glad to acknowledge my friends who work in my research group. First, I would like to thank Sergiy Peleshanko for offering his help with purification of chemicals for this research. Thanks to Sergiy Markutsa for helping with high-resolution AFM imaging of MscL. Thanks to Jason Holzmueller for help with contact angle measurements. My special thanks to Kirsten Larson Genson, Melburne LeMieux, Duangrut Julthongpiput, Nobumishi Fushigami for sharing with me their hands-on research experiences.

I would also like to acknowledge collaboration with Dr. Morly Stone and Sharon Jones (AFRL) and for guidance and valuable discussions in the protein study as well as for providing me with MscL protein sample. I would like also thank Dr. Hagan Bayley (Taxas, A&M) for supplying hemolysin samples. Thanks Dr Paul Blont (Southwestern University,TX) and for spending time in useful discussions and guidance.

Thanks also to my POS committee for all their guidance and time they have devoted to my thesis presentations. Special thanks to Dr. Vladimir Tsukruk, my major professor, for patience, support and guidance during my Master degree.

I would like to gratefully acknowledge funding from the Air Force Office of Scientific Research, Contracts F496209810480 and F496200210205.

ABSTRACT

The major goal of this research is to understand design principles of interfaces, suitable for the reconstitution the ion channel membrane proteins. In the present work, we focused on immobilization of two channel proteins, staphylococcal α-hemolysin and Mechanosensitive Ion Channel of Large Conductance (MscL) from Salmonella typhimurium, onto single crystal silicon substrates. High-resolution atomic force microscopy (AFM) was utilized as a tool for the monitoring of the molecular conformations of the ion channels after immobilization. As observed, α-Hemolysin was adsorbed onto bare silicon in collapsed state, while adsorption of MscL resulted in unraveling of the protein. LB deposition of proteins embedded in lipid monolayer reduced denaturation of the proteins on silicon surface, due to reduced surface energy. Octedecyltimethoxy silane (ODTMS) self-assembled monolayers (SAMs) were used as a "buffer layer analog" of a lipid membrane. MscL was successfully reconstituted in these organic SAMs. Analysis of dimensions of the MscL displayed that the gating state and the molecular conformation of SAM-supported MscL can be controlled by variation of the surface energy of the supporting surface layer. Closed, intermediate, and open states were observed on surfaces with different surface tensions. Obtained results demonstrated an agreement with known molecular modeling data for gating mechanisms of the MscL protein in lipid membrane.0

CHAPTER 1. ADVANCES IN IR SENSOR DEVELOPMENT

In many applications, it is necessary to measure temperature of an unattainable object. Lightweight, compact, and easy-to-use, IR thermometers can safely measure hot, hazardous, or hard-to-reach surfaces without contaminating or damaging the object. At the same time, infrared thermometers can provide several readings per second, as compared to contact methods where each measurement can take several minutes.

Recent advances in microelectronic technologies have led to bulk production of silicon fabricated IR microsensors.[1] Silicon sensors/systems provide extremely high accuracy, very compact size, and excellent corrosion resistance. A silicon single crystal will not undergo plastic deformation and stays perfectly elastic until it breaks. Therefore, silicon-based sensors do not suffer from fatigue and hysteresis problems.

However, the rigidity of silicon limits minimal spatial dimensions of a micromachined IR sensor and therefore its resolution. It is the reason of a narrow range of detection and tuning problem of the once made silicon chip. In the development of the microsensor technologies, several different components have to be optimized. A complete sensing system should have perfect information sensing, information processing, and actuating.

Major driving force in biomimetic research and development of IR sensor devices is achieving the miniaturization and high performances comparable to that of biological systems. One could find in nature an amazing collection of specially evolved sensory

apparatus. Biomimetic approach in sensor design targets unique microstructures and specific properties of the biological thermal receptors. Biological IR sensors are operated in ambient conditions, and their sensitivity is by two orders of magnitude higher than sensitivity of any known man–made IR sensors.[2]

Recent studies have shown that IR organs of venomous snakes and fire beetles may be the most sophisticated infrared sensors in nature.[3,] Anatomically, biological IR-sensitive elements are represented by arrays of free-suspended elastic thin film membrane structures. Measured deflection of a single thin-diaphragm upon IR adsorption gives one pixel to an IR image. It was found that molecular mechanisms of biological IR detection involve pressure-modulated ion channel proteins.[4] These channels are triggered by strain in membrane caused by deformation of IR-absorptive tissue. Some bacterial ion channels serve as reporters of strain in lipid membranes. These proteins are considered prospective models for design of a new generation of highly sensitive, lightweight, thermal sensors, capable of the operating in the ambient conditions.

In this spirit, the current study is aimed to design the synthetic/biomacromolecular/inorganic film assemblies, which could be used as a sensitive element of a thermal sensor. This research is concerned with elucidation of optimal conditions for immobilization of two bacterial channel proteins: mechanosensitive protein of large conductance (MscL) from *Salmonella typhimurium*, and α-hemolysin from *Staphylococcus aureus*. The proteins are deposited onto silicon, and onto alkylsilane self assembled monolayers (SAMs). Several techniques are tested for the immobilization of the

proteins: Langmuir-Blodgett (LB) transfer, liposome fusion, and adsorption. Microstructure and conformations of the reconstituted ion channels are characterized with atomic force microscopy (AFM) to ensure that the macromolecular assemblies preserve intact conformation of proteins.

CHAPTER 2. CRITICAL LITERATURE REVIEW

2.1. Infrared thermometers

Non-contact temperature sensors are based on the principle that all objects warmer than absolute zero (0°K) emit energy in the range of wavelengths between 0.7 and 1000 μm of the electromagnetic spectrum. IR thermometers are able to determine object's temperature without touching it by measuring the amount of IR energy being emitted from the object. Basic components of an IR thermometer are shown on Figure 1.[5] The lens collects energy emitted from the object. Detector converts thermal energy to electrical signal. Usually the detector also serves as signal filter and amplifier. The measured temperature of an object is determined from the detector temperature. For this type of thermal sensor it is very important that the internal temperature must be known and kept constant after calibration.

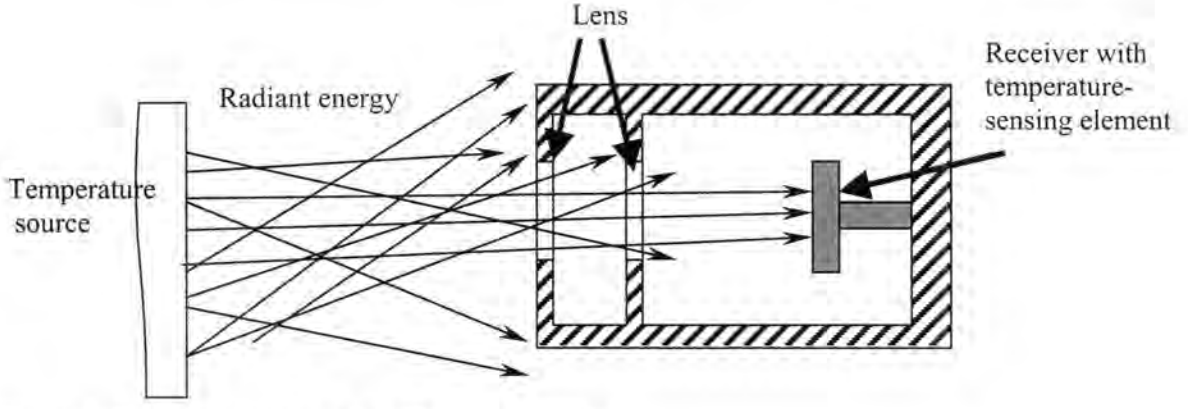

Figure 1. Basic components of an IR thermometer.[5]

The detector should be highly sensitive because only a small portion of emitted IR radiation reaches the detector. Common types of infrared sensors are thermopiles,

bolometers, and Golay cells.[5] The Golay photo-thermal cell was introduced in 1947. [6] The relative advantage of the Golay cell over other types of detectors is a wide range of detected wavelength and comparatively high sensitivity. The Golay cell uses detection of sub-micrometer-scale deviations of a flexible membrane caused by gas expanding in a sealed rigid cell. [7,8] Radiation absorbed by a receiver inside a gas-filled chamber heats the gas, causing its pressure to rise, which displaces a flexible membrane upon which a mirror is mounted. The movement of the mirror produces a change in the photocell current.

The micromachined version of the Golay cell has been recently proposed (Figure 2). A sensing element is composed of a solid silicon membrane with thickness close to 1 micron.[9] The membrane seals a gas-filled cavity. In a non-stressed state, electrostatic force pulls the membrane into contact with the tip of the deflection electrode. With the absorption of infrared radiation, the pressure in the trapped gas changes. The feedback circuit responds by modifying the deflection voltage. The prototype sensor performed repeatable measurements at ambient temperature, 300K. However, it was reported that linear response was limited to small temperature difference, ±0.2 K. This limitation should be associated first of all with rigidity of the silicon membrane.

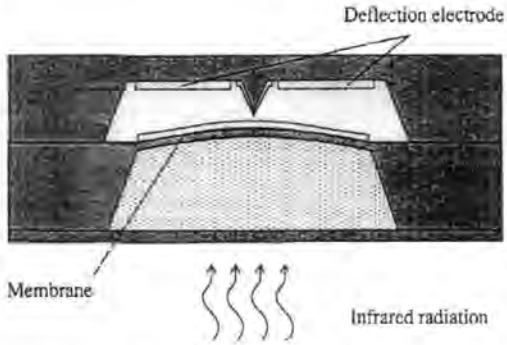

Figure 2. Diagram of a micromachined infrared sensor based on tunneling detection. [9]

The sensitivity of diaphragm depends on its geometrical parameters and material properties. Figure 3 indicates the relationship between sensitivity and diaphragm thickness of a micromachined membrane pressure sensor. In the Figure 3, the sensitivity increases from 0.6 to 3.75mV/V psi when the diaphragm thickness reduced from 52 to 8 μm. This is in an agreement with the fact that bending rigidity of the plate with a uniformly distributed load is proportional to the cubed thickness of the plate as given by equation 1:

$$D = \frac{Eh^3}{12(1-\nu^2)} \quad (1)$$

where h-is the thickness of the plate, E is Young's modulus, and ν- is Poisson's ratio of the plate material.

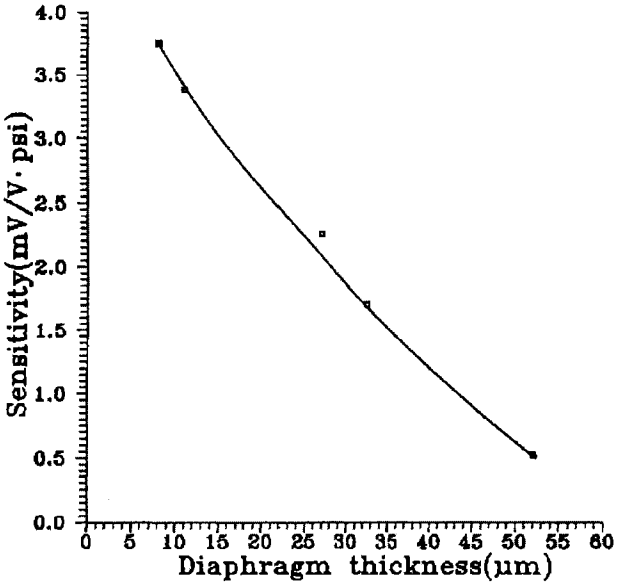

Figure 3. Sensitivity versus various diaphragm thicknesses.[10]

This relationship indicates that the performance of such type of membrane sensors should benefit from further miniaturization. However, minimal sizes of micromachined silicon membrane structures is limited to 800 μm in lateral dimension and 1 μm in thickness, because of brittleness of silicon materials. [11] This limits further miniaturization despite the fact that decrease of thickness from 1 μm to 10 nm would increase sensitivity by six orders of magnitude.

2.2. Biological IR-sensory systems.

Examples for miniaturized membrane strain sensors are found in nature. Numerous studies of biological IR receptors give insights to their structure and comon physical

processes involved in biological thermal detection. [12,13,14,15] It is now considered that IR detection in various species is based on the thermo-mechanical principle. [16,17,18,19]

The thermo-mechanical principles of thermal detection in snakes has been studied in detail. The infrared organs are organized arrays of pits; each pit is a single IR sensor.[3] A single IR sensor of *Crotaline* snake consists of an inner and outer chamber separated by a thin (15 μm) elastic membrane that contains the receptor terminal nerve masses (Figure 4). A small elastic membrane is surrounded by insulating layers of air. This provides an ideal site for rapid localized heat absorption and thus stimulation of receptors (free nerve endings that are present). Upon absorption of infrared radiation, the tissue expands and exerts compressive forces on the dendritic tip. It is suggested that the deformation of the tip on the order of 0.1 nm causes firing of a primary neuron.[13]

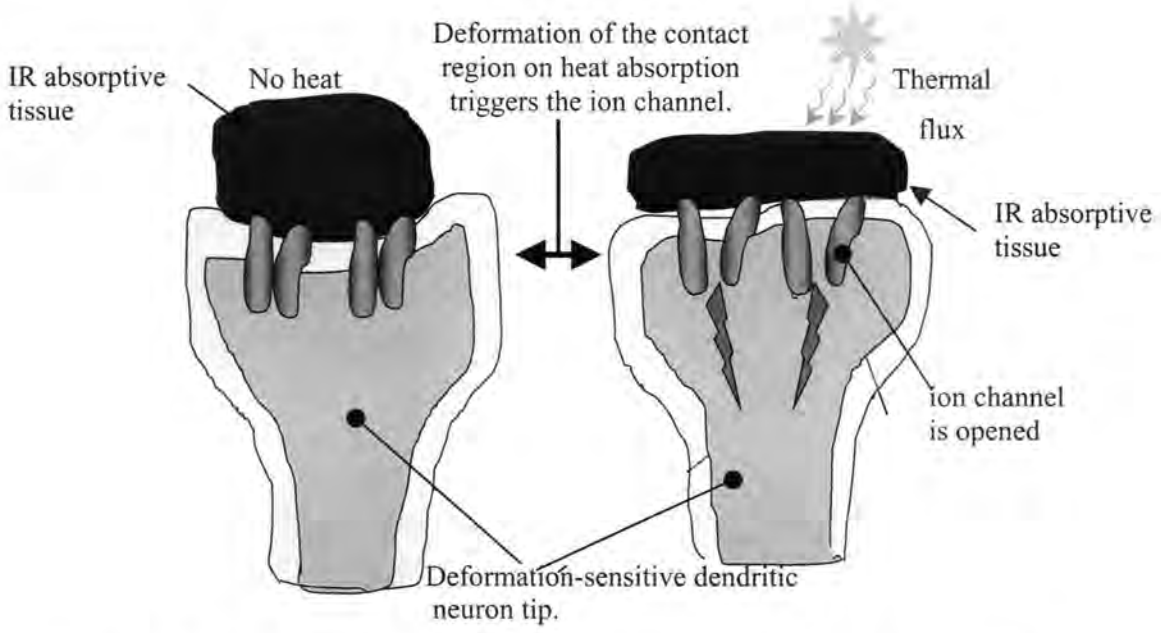

Figure 4. Diagram, showing stimulation of thermoreceptive neurons by thermal flux.

It is believed that IR-induced neural impulse originates in specific ion channels located in a neuron cell membrane. Biochemical studies have revealed calcium-regulated ion channels in the outer membrane of the thermosensing neuron in pythons. [14] In-vitro studies of this channel are not been completed , but the structure of this ion channel is similar to so called volume-regulated ion channels (VR1 and VRL-1), which have been found in mammals. These volume-regulated ion channels open and close in neurons in response to mechanical stimuli, which cause sense of touch and hearing. [20] Therefore it is suggested that a similar transformation of the mechanical deformation into an electrical signal is performed in biological IR receptors.

2.3. Stress-modulated ion channels

In mammals, a diverse range of stress-modulated ion channels are involved in a number of important physiological processes, such as touch sensing, hearing, and balance.[11] Bacteria do not have neurons, but they do contain a variety of ion channels. However, only few ion channel proteins are able to response to physical stimuli. These integral membrane proteins enable rapid diffusion of ions through transmembrane pores. A key feature of such pores is that they are 'gated', i.e. they are not always open, but instead switch between open and closed conformations in response to specific changes in the surrounding.

These so-called mechanosensitive ion channels are considered a prospective sensing element for stress-actuated sensors. MscL from *Mycobacterium tuberculosis*, in native state is gated by local stresses in cell membranes, serving as an osmotic gauge protecting cells from hypotonic shock by reducing intracellular pressure through release of cytoplasmic osmolytes (Figure 5).[21,22] MscL homologues from different microorganisms are being studied as model for how a protein senses and responds to membrane tension. [23,24] When MscL from *M. tuberculosis* or *E. col,* is re-solubilized and reconstituted, it yields wild-type channel currents in patch clamp.[25,26] The structure of such proteins was studied by X-ray diffraction with a resolution of 0.35 nm.[27] Electrophysiological studies reveal that MscL, in the open conformation, has a pore size of 3 nm. [28] This represents an enormous conformational change and means that MscL are capable of passing large macromolecules.

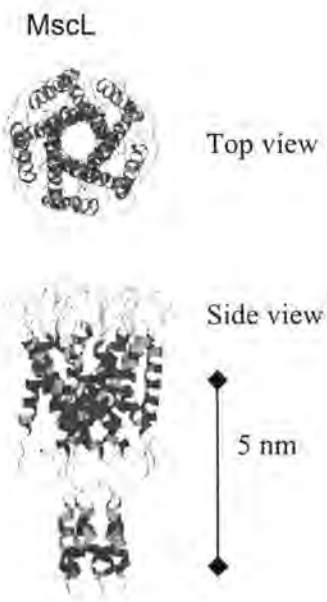

Figure 5. Structure of MscL from *Mycobacterium tuberculosis.*[16]

Pressure-gated ion channels are elements of the cell's adaptation mechanism for osmotic stress. They control a response that protects the bacterial cell from lysis*. It is a well known fact that lipid vesicles behave osmometrically, that is, water diffuses across the membrane in response to the osmotic difference between the inner compartment and the outside medium. The diagram on Figure 6 demonstrates how a cell without compensative

* Lysis is a rupture of the cytoplasmic membrane causing death of the bacterial cell.

mechanism undergoes lysis, whereas cell with mechanosensitive ion channels can lower internal pressure by releasing intracellular components. When osmotic pressure inside the cell exceeds a safe limit, mechanosensitive channels open and release a portion of cytoplasmic ionic compounds. In this manner, the cell equilibrates pressure across the plasma membrane before lysis.

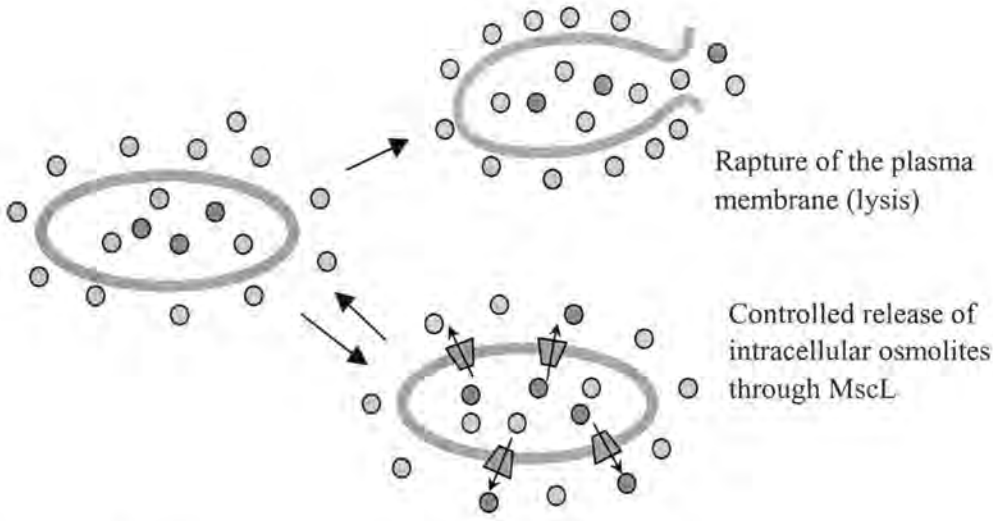

Figure 6. Effect of osmotic downshift shock on cell membrane.

Opening of MscL ion channel is triggered by structural changes in membrane. Osmotic downshifts in cytoplasm lead to relative increases in membrane area and decreases in membrane thickness and curvature changes. Recent studies of the bacterial mechanosensitive channel proteins have combined a number of different approaches to come up with a model for the channel gating mechanism. [22,29] A putative gating mechanism has been derived from electrophysiological studies in combination with molecular modeling. This model suggests that significant shape change of the channel is the result of iris-like transition with change in tilt of helical domains (Figure 7). The diameter of the channel is

increased from 0.4 nm in closed state to about 4nm in opened state. Significant expansion of the channel in lateral direction is accompanied by decrease in height of the protein molecule. Electrophysiological experiments and molecular modeling allowed predicting several intermediate states, discriminated by an increase of overall diameter and decrease in heights of the molecule.

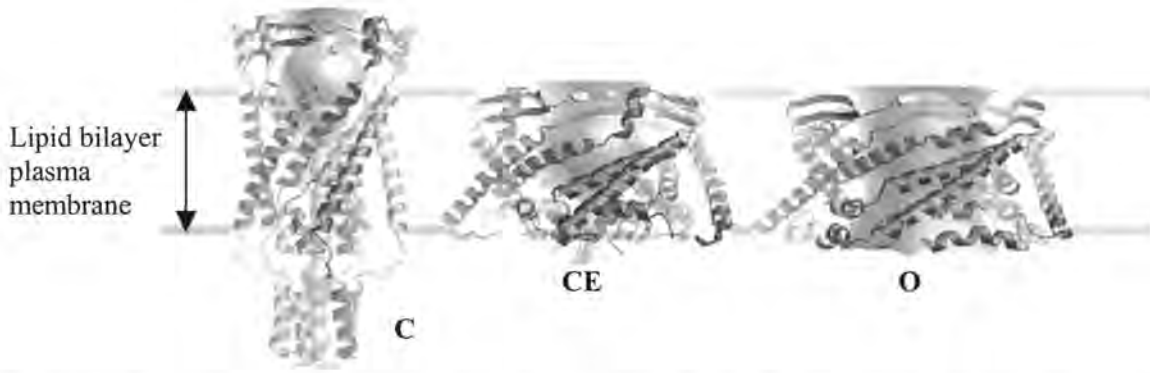

Figure 7. Molecular graphics images of the MscL channel in closed (C), closed-expanded (CE) and open (O) states.[29]

Staphylococcal α-hemolysin is another attractive candidate for biosensor design (Figure 8). The structure of α-hemolysin is somewhat similar to MscL, and low cost of its purification is advantageous compared to most pore forming proteins. [30] α-Hemolysin is a toxin, produced by the bacteria *Staphylococcus aureus* and is secreted as a water-soluble polypeptide. [31] It was demonstrated that oligomeric staphylococcal peptide molecules with molecular weight of 33.2 kDa, assemble in heptameric α-toxin pore within the cell membrane. Each oligomer undergoes changes in its secondary structure that result in exposure of hydrophobic regions in the vicinity of lipid membrane. This pore protein

contains a large central channel (2 nm) that can be altered by gene engineering and chemical methods, giving the protein new abilities of specific recognition. [32,33,34]

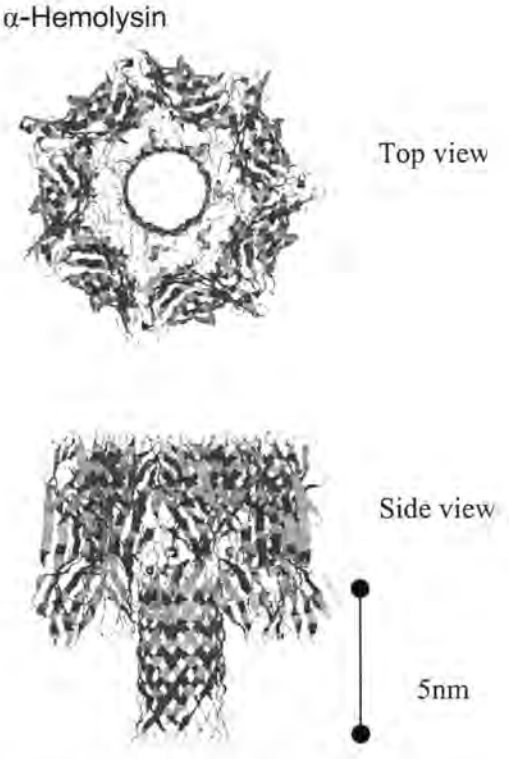

Figure 8. Structure of α-toxin from *Staphylococcus aureus*.[25]

The heptametrical hemolysin complex is solubilized with detergents in water. Knapp et al. showed that even though conformation of α-toxin channel upon solubilization with detergents is different from the conformation within the native membrane environment, the channel is capable of reconstitution in lipid membranes. [35]

Using data provided in Table 1, we can compare properties of model channels used in this research. The MscL channel is gated by pressure change within lipid membrane. α-hemolysin is a nonselective ion channel; the pore is permanently open from the moment

when protein aggregates on the host membrane. The two channels have a different ratio of hydrophobic-hydrophilic amino acids and therefore a distinct orientation within natural lipid membrane.

Table 1. Overview of structural characteristics of MscL and α-hemolysin .

Name:	**α-hemolysin** [***Staphylococcus aureus***]	**MscL** [***Mycobacterium tuberculosis***]
Chains	7 (Homo heptamer)	5 (Homo pentamer)
Molecular weight, Mw	231 kDa	58 kDa
Number of aminoacids	2 051	545
Crystal dimensions, a-b-c	10-10-10 nm	5-5-8 nm
Secondary structure	Alpha 0% Beta 60%	Alpha 48% Beta 0 %
Hydrophobic aminoacids	40%	70%
Matthews coefficient, VM	$3.0 \cdot 10^{-3}$ nm^3/Da	$5.98 \cdot 10^{-3}$ nm^3/Da

The structure of membrane proteins is stabilized mostly via balance of hydrophilic and hydrophobic interactions. MscL has remarkably high percentage of hydrophobic amino acids in the sequence. In native state, MscL is almost completely submerged into the hydrophobic vicinity of a lipid bilayer. Hemolysin, on the other hand, is composed of 60% hydrophilic amino acids. This protein is incorporated into a membrane only about 20% of the total sequence would be interacting with hydrophobic part of a lipid bilayer (see Table 1).

2.4. Sensing stress in cell membrane

The triggering mechanism for gating of MscL is still under discussion. It is assumed that the lipid membrane mediates the gating of the protein.[36] It was shown that the signal is transduced via alterations in the protein-lipid interactions rather than direct sensing of ion concentration by the proteins. [37] However, there are still differing opinions regarding the triggering parameter. The most often discussed factors are: the change in the bilayer thickness, the hydrophobic mismatch; the membrane asymmetry; the membrane curvature, the lateral pressure in the membrane and the interfacial energy. [37]

Some models of stress in the lipid membrane are based on the assumption that the lipid bilayer behaves as an elastic solid. According to this model, the intrinsic mechanical properties of the membrane can be described by four elasticity moduli that characterize the response of a unit area of bilayer to volume compression, area expansion, bending/curvature and extension/shear. [38]

A common experimental setup for MscL study involves deformation of a bilayer lipid membrane (BLM) patch suspended over a pipette tip. Upon applied pressure, the planar lipid bilayer or lipid vesicle responds to mechanical deformation by elastic membrane dilation/thinning and curvature changes. [38] Localized changes in bilayer thickness and curvature lead to increase ion transport through the channel, which results in conductivity changes.

Perozo et al. have studied the effect of asymmetry in a bilayer lipid membrane (BLM) on functioning of MscL. The changes in membrane curvature were induced by adding lysophosphatidylcholine (LPC) to the external leaflet of BLM. As a result MscL displayed a dramatic increase in single-channel activity even in the absence of applied pressure, which means that the channel was trapped in the fully open state. The obtained results demonstrate that the asymmetry in the lateral pressure between the two lipid monolayers causes to opening of the channel. [39]

The same group investigated influence of the lipid thickness on MscL function. [40] It was found that decreasing bilayer thickness lowered MscL activation energy. Although hydrophobic mismatch alone was unable to open the channel, it probably can be used to stabilize the open conformation of MscL.

2.5. Protein immobilization

Choice of immobilization technique depends on specific properties of the protein. The best method of immobilization should guarantee that the immobilization layer does not inactivate biomaterials. For example, it is possible to attach most proteins chemically to the substrate but it may chemically modify the binding sites and denature the molecules.[41] There are several possible modes of physically coupling the biomolecules to the basic solid substrate: membrane entrapment, physical adsorption, matrix entrapment, and covalent attachment to the surface. [42]

Membrane channel proteins are ruled by balanced hydrophilic and hydrophobic interactions. Therefore, these molecules are subjected to local stresses during transfer and deposition processes. It is a challenge to effectively utilize a channel protein out of its natural lipid environment. Preservation of conformational mobility and intact gating capability is critical for protein functioning in an artificial environment. Unbalanced protein-surface interactions result in eventual unfolding of the channel protein molecules with complete loss of activity. Therefore establishing an immobilization procedure is a critical step in the design of prospective silicon nanosensor devices based on biomacromolecular sensitive layers with ion channels.[43,44]

Immobilization of membrane proteins often relies on non-specific adhesion mechanisms, such as hydrophobic interactions to anchor the molecule to the substrate. Previously, several different strategies have been exploited to fabricate protein-lipid organized monomolecular films on solid substrates.[45] It was observed that direct deposition of lipid-protein layers on a bare silicon dioxide surface of glass and quartz resulted in loss of protein mobility due to excessive interactions with substrate beneath the lipid bilayer. Spontaneous self-assembly and a Langmuir-Blodgett (LB) deposition were used to implement this approach. Shen et al. demonstrated that under certain conditions, dewetting processes could be suppressed and uniform lipid-polymer films could be obtained with an appropriate level of lateral diffusion. However, the lipid-based films created this way are not stable against external stresses and disturbances due to their weak physical interaction with the solid surface.

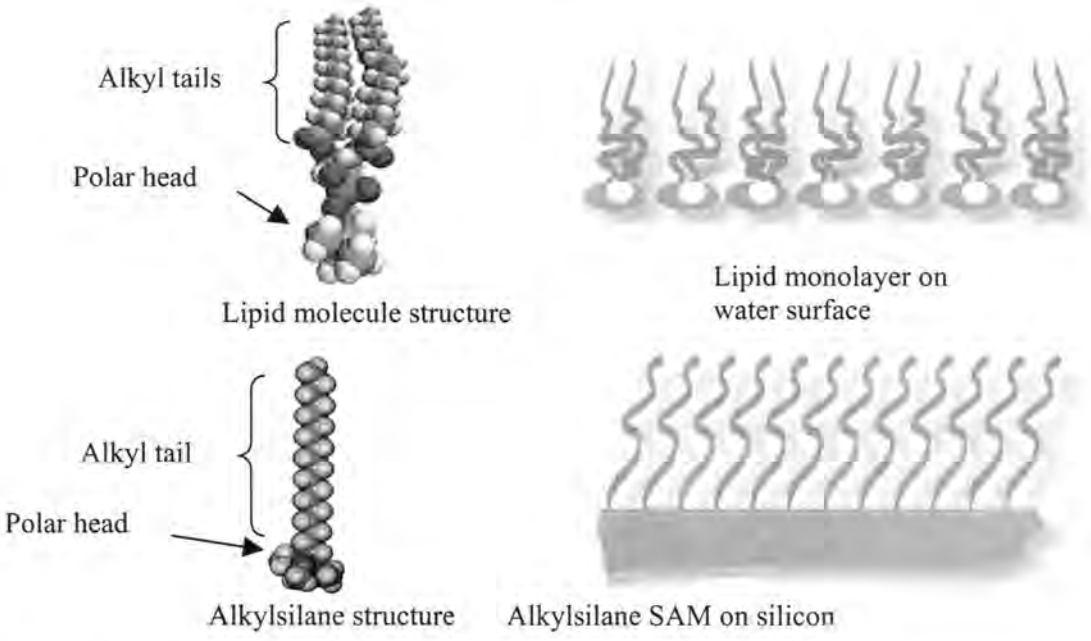

Figure 9. Schematic of lipid monolayer and alkylsilane SAM.

A number of other approaches to immobilize membrane proteins have been proposed. Various fabrication schemes include LB, spontaneous fusion of lipid vesicles on un- or pre-coated surfaces, and self-assembled, tethered lipid mono or bilayers. [46,47] All these techniques deal with natural lipids, or lipid like molecules. Alkyl-silane SAMs are frequently used as a lipid monolayer imitation.[48] They have structural properties similar to lipids. Alkylsilanes have the general formula $RSiX_3$, where R is alkyl, and X is Cl or methoxy ($-OCH_3$) groups. SAMs of alkylsilanes with long alkyl tail (C18) may serve as a substitute of lipid layer for membrane proteins. Figure 9 shows resemblance of lipid monolayers and alkylsilane SAMs. Alkyl-silane self-assembly technique is a primary choice for immobilization of membrane proteins onto silicon surfaces. This versatile tool enables variation of molecular structures on the surfaces with different deposition techniques, and a variety of silanes available on the market.

CHAPTER 3. GOAL, OBJECTIVES, AND APPROACHES

3.1 Goal

The aim of the research is to incorporate ion channel protein into an artificial matrix attuned with silicon microelectronic devices. The prime criteria of a good compatibility of a protein and synthetic organic layer is the similarity of the observed molecular structures of the proteins in comparison to the known parameters of the proteins' crystal structures. This study is concerned with immobilization of two ion channel proteins: MscL from *Salmonella typhimurium* and α-hemolysin from *Staphylococcus aureus*. The model organic layers are composed of natural lipids (phosphatidylcholine, cholesterol), and synthetic amphiphilic molecules (alkylsilanes). The influence of immobilization procedures and structure of synthetic matrix on molecular conformation of the proteins is examined. AFM, ellipsometry, and contact angle measurements are employed to study the solid supported layers.

3.2 Objectives

- To fabricate several types of SAM-modified substrates for channel protein immobilization.
- To characterize surface properties of the SAMs.
- To compare the microstructure of the Langmuir-Blodgett (LB) and absorbed protein-incorporating layers on a silicon support using AFM.
- Evaluate and optimize the procedure to provide conditions of structural integrity of the reconstituted ion channel proteins immobilized on the surface.

3.3 Approaches

The focus of the research is on structure (conformation) of the protein molecules immobilized in different substrates to assure compatibility of the protein with a solid matrix. Our approach to reconciling the contradictory requirements of a supported yet unconstrained channel protein is to produce a system which mimics the natural balance of lateral interactions in lipid membranes, so that the protein is associated with the substrate but is still functional. Preservation of conformational mobility and intact gating is critical for functioning in an artificial environment.

Molecular structures of the proteins are known from X-ray crystallography studies. These structures should be taken as a reference for comparison with experimentally observed conformations. As a model matrix for channel protein immobilization, we are going to use silane SAMs with variable density of grafting.

CHAPTER 4. MATERIALS AND METHODS

4.1. Materials

Chemical structures of several types of surfactants which are used in this research for fabrication of SAMs are presented in Figure 10.

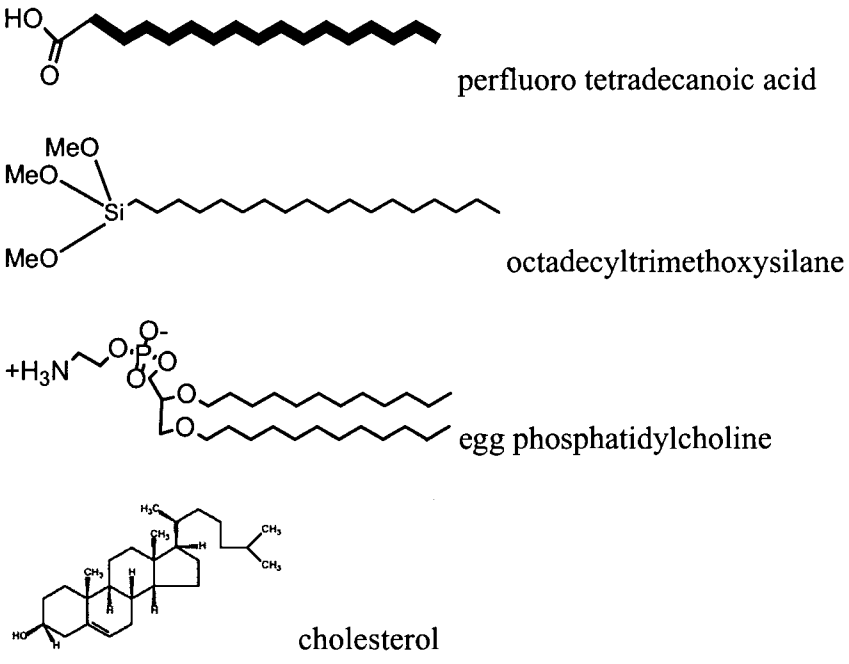

Figure 10. Chemical structures of surfactants used in this research.

Egg phosphatidylcholine and cholesterol are purchased from Avanti Polar Lipids and used as received. Octadecyltrimethoxysilane (ODTMS) and octadecyltrichlorosilane (OTS) are purchased from Aldrich. Perfluorotetradecanoic acid (PFTDA) is purchased from Alfa-

Aesar. Organic solvents HPLC grade (chloroform, hexane, and toluene) from Fisher Scientific are used as received. All water solutions are prepared using purified water (Nanopure, >18 MΩ· cm). Sulfuric acid, 98% of reagent grade, and hydrogen peroxide, 30% of reagent grade (Fisher Scientific), are used for pre-fabrication treatment of silicon wafers.

Staphylococcal α-hemolysin heptameric pore was obtained from H. Bayley, Texas A&M University, and used as received.[49] MscL from *Salmonella typhimurium* was purified as described by Jones et al.[50] Overnight culture of *E. coli* [courtesy of Dr. Morley O. Stone, Air Force Research Laboratory, Wright Patterson AFB] strain is harvested by centrifugation at 5000rpm. Cell pellet is resuspended in 10mM Tris pH7.5 buffer, with 10nM NaCl, and 1.5% dodecyl maltose (DDM, Aldrich hemolysin 86231-2). After incubation for 30 min in water bath at 37°C the suspension is sonicated on ice for 2 min. The sample was clarified by centrifugation at 25000 rpm, at 4°C, for 10 min. MscL was adsorbed onto TALON resin (Clontech hemolysin 8801-1). After several extractions with 50mM Sodium Phosphate and 300mM NaCl buffer the protein is eluted with buffer containing 1M imidazole. The protein solution was dialyzed against 10mM NaPO4 buffer pH7.4 overnight. Sorption onto Talon Resin and dialysis cycle was repeated 2-3 times, until protein homogeneity in SDS page. Protein concentration in purified sample is quantified using Bio-Rad assay kit (hemolysin 500-0002). MscL solution is stored in a refrigerator at 4°C.

4.2. Sample fabrication

4.2.1. Silicon substrate preparation

The solid substrates are freshly cleaned, atomically smooth, [100] silicon wafers of high quality surface with micro roughness not exceeding 0.1 nm within 1x1 μm surface areas (Semiconductor Processing Co). Silicon wafers are cut in rectangular pieces of ~1×2 cm. Wafers are cleaned to remove any organic and inorganic contaminants from the surface according to the standard procedure.[51] Initially, silicon wafers submerged in Nanopure water are treated for 10 min in an ultrasonic bath at room temperature. Then, they are cleaned with a hot "piranha solution" (30% concentrated hydrogen peroxide, 70% concentrated sulfuric acid, *hazardous solution*!) for one hour to remove organic contaminants and strip original silicon oxide surface layer. Finally, treated substrates are abundantly rinsed with Nanopure water and dried with a dry nitrogen stream. This treatment results in a fresh silicon oxide layer of 1.2-1.4 nm thick with a high concentration of silanol groups accessible for further chemical reaction.

4.2.2. Preparation of homogeneous ODTMS SAMs

The fabrication of homogenous ODTMS SAMs is conducted according to the known chemisorption procedure. [52,53] The routine is conducted in a dry nitrogen glove box, and under a clean-room 100 conditions. Freshly cleaned and dried silicon wafers are dipped in 1% (w/w) solution of ODTMS in anhydrous toluene for chemisorption. After that, wafers are rinsed 3 times with chloroform and dried in air. Samples with controlled density of grafting are made by changing time of adsorption. Variations in surface density are achieved by applying different times of adsorption (from 10min to 12 hours).

4.2.3. Preparation of ODTMS pattern via LB deposition

Patterned hydrophilic-hydrophobic surfaces are fabricated via LB-deposition of mixed monolayers of ODTMS and PFTDA. Dilute chloroform solution (1 mmol per liter) of ODTMS and PFTDA with 4:1 molar ratio was deposited using LB technique on an R&K-1 trough (Riegel & Kirstein, GmbH) at constant speed 1mm/sec.[54] Deposited mixed monolayer is cured at 60°C in vacuum oven for 1 hour to assure chemical tethering of ODTMS. After incubation, the wafers with deposited mixed monolayers are rinsed with chloroform to remove PFTDA. As a result, physically adsorbed phase-dispersed PFTDA is dissolved, thus exposing bare silicon areas surrounded by chemical grafted ODTMS monolayers (Figure 11). Patterned substrates are dried in the air. Dry substrates are used for protein immobilization.

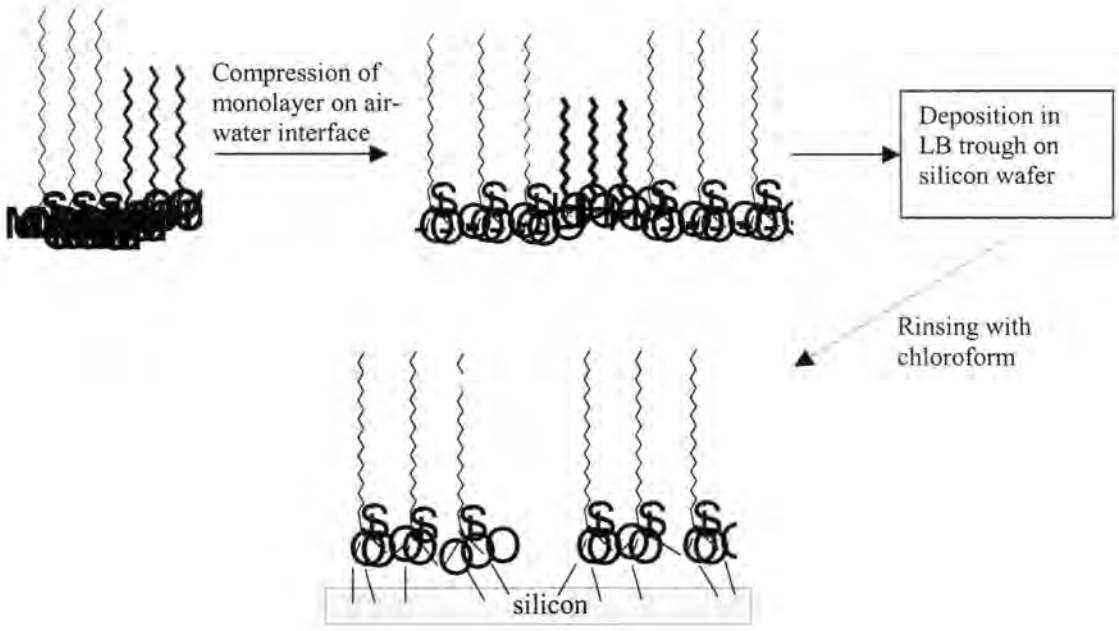

Figure 11. Scheme of fabrication of ODTMS pattern through mixed LB layer deposition.

4.3. Protein incorporation techniques

4.3.1. Mixed lipid-protein LB monolayers

Mixed lipid protein monolayers are prepared using LB technique (Figure 11). Lipids are dissolved in chloroform to obtain dilute solutions with concentration of 1 mmol/L. Chloroform lipid solutions are spread on the Nanopure water surface and left to evaporate for 20 minutes.

Than, the protein solution is injected into the water sub-phase. For Hemolysin reconstitution in lipid, 20μl of solution of the protein was injected by a microsyringe into the water sub-phase. For MscL protein reconstitution into lipid monolayer, the liposome fusion technique was used.[55] 200μl of MscL-liposome mixture in water was injected by a microsyringe in a water sub phase. Liposomes and protein were allowed to fuse with lipid monolayer for 20 minutes. Fusion of liposomes containing membrane protein with lipid monolayer is shown in Figure 12.

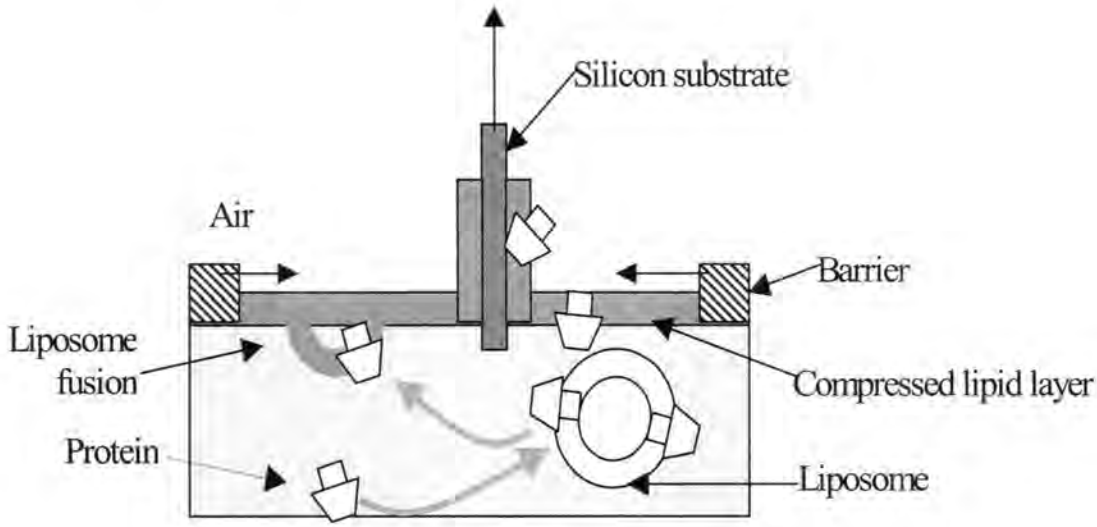

Figure 12. Schematic LB deposition of lipid-protein mixed monolayer and liposome fusion.

Finally, the monolayers are compressed to 30 mN/m and deposited on a freshly prepared silicon substrate at constant speed of 1 mm per second. The surface pressure is held constant as the submerged silicon substrate is lifted from the trough. Deposited LB monolayers are characterized with AFM emidiately after transfer to a solid substrate.

4.3.2. Protein adsorption

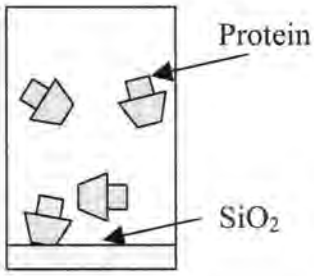

Figure 13. Schematic of protein absorption onto silicon substrate.

Samples with protein adsorbed onto bare or modified silicon surfaces are prepared by applying a 20 μl droplet of protein solution on a substrate (Figure 13). After one-minute exposure, the substrates were rinsed with 1 ml of Nanopure water to remove excess protein.

4.3.3. Preparation of proteo-liposomes

Protein-liposome solution for ion channel protein reconstitution is prepared as described by Bayley et al.[56] 0.5 ml chloroform solution (1mg/ml) of lipid (egg phosphatydilcholine or its 1:1 molar ratio mixture with cholesterol) is quickly dried in a tube under dry nitrogen. Then, 10 ml of Nanopure water is added to the tube with dried lipid-protein mixture. The tube is placed in the ultrasonic bath for 15 minutes. 20μl of MscL protein solution is added to 200μl liposome solution and allowed to interact with liposomes for 1 hour in a refrigerator (4°C). After sonication, the obtained protein-liposome solution is used for deposition via LB technique, or for adsorption onto a solid substrate.

4.4. Characterization techniques

4.4.1. AFM

AFM provides a unique opportunity for visualizing biological macromolecules in three dimensions on a nanometer scale. Under optimum conditions AFM is capable of resolving surface detail down to the atomic level. [57] Typical AFM setup is shown on Figure 14. Microfabricated silicon cantilevers with sharp pyramidal tips are used for the AFM studies. The scanning cantilever is mounted under a piezo tube that is used to move the tip over the sample.

The laser beam is focused on the cantilever. The reflection of the laser light is projected via a mirror onto a quadrant photodiode. The difference in the intensity between the left and the right half of the detector is proportional to the cantilever deflection and is a measure for the tip position. An image is obtained while the tip is raster-scanned over the sample. At each position, the cantilever deflection is measured, and thus a topography map can be constructed.

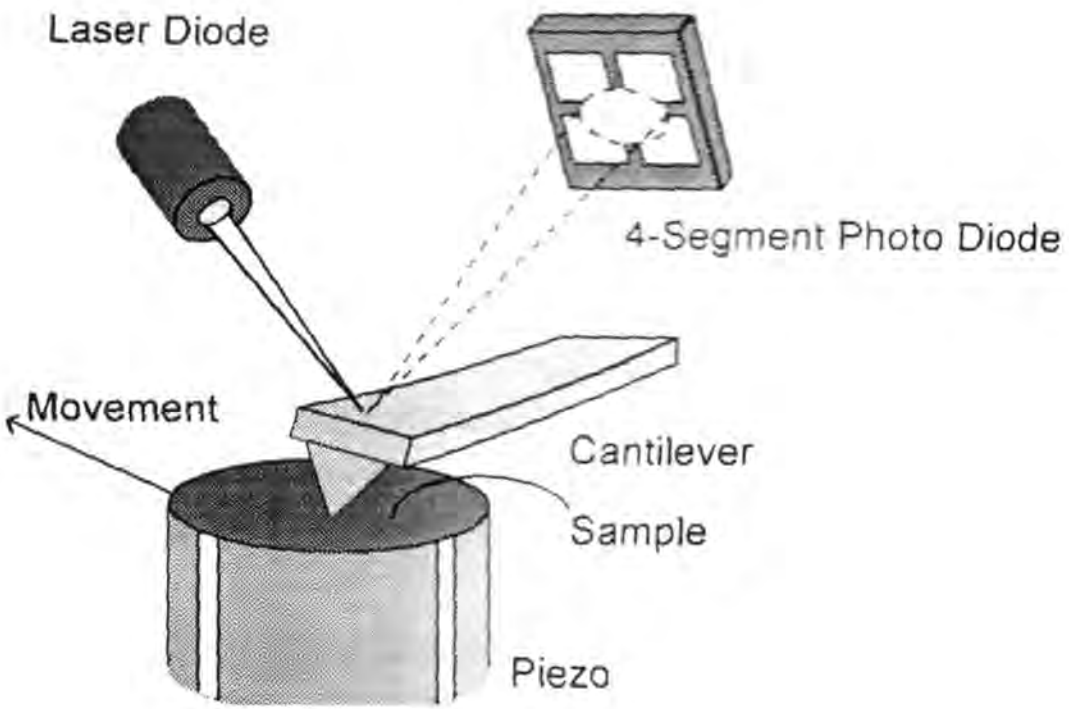

Figure 14. Atomic Force microscope setup.[58]

The laser beam is focused on the cantilever. The reflection of the laser light is projected via a mirror onto a quadrant photodiode. The difference in the intensity between the left and the right half of the detector is proportional to the cantilever deflection and is a measure for the tip position. An image is obtained while the tip is raster-scanned over the sample. At each position, the cantilever deflection is measured, and thus a topography map can be constructed.

AFM imaging of fragile samples like individual molecules puts high demand on the measurement. The first complication of AFM imaging of individual molecules is tip-induced

surface damage. For reproducible imaging of molecules, the interaction forces need to be controlled carefully to prevent damage. A reduction of lateral forces can be achieved using *tapping mode*.[58] In this mode, the cantilever is oscillated at its resonance frequency. The tip is lowered until it approaches the surface, and due to the interaction with the surface the tip amplitude decreases (Figure 15).

Amplitude is kept constant by a feedback loop, and the feedback signal is used for imaging. In this way, the tip-sample contact time is limited to a very short period during impact, and as a result, frictional forces are negligible compared to the normal forces. For biological applications, tapping mode operation is preferable because of the reduction of tip-induced damage.

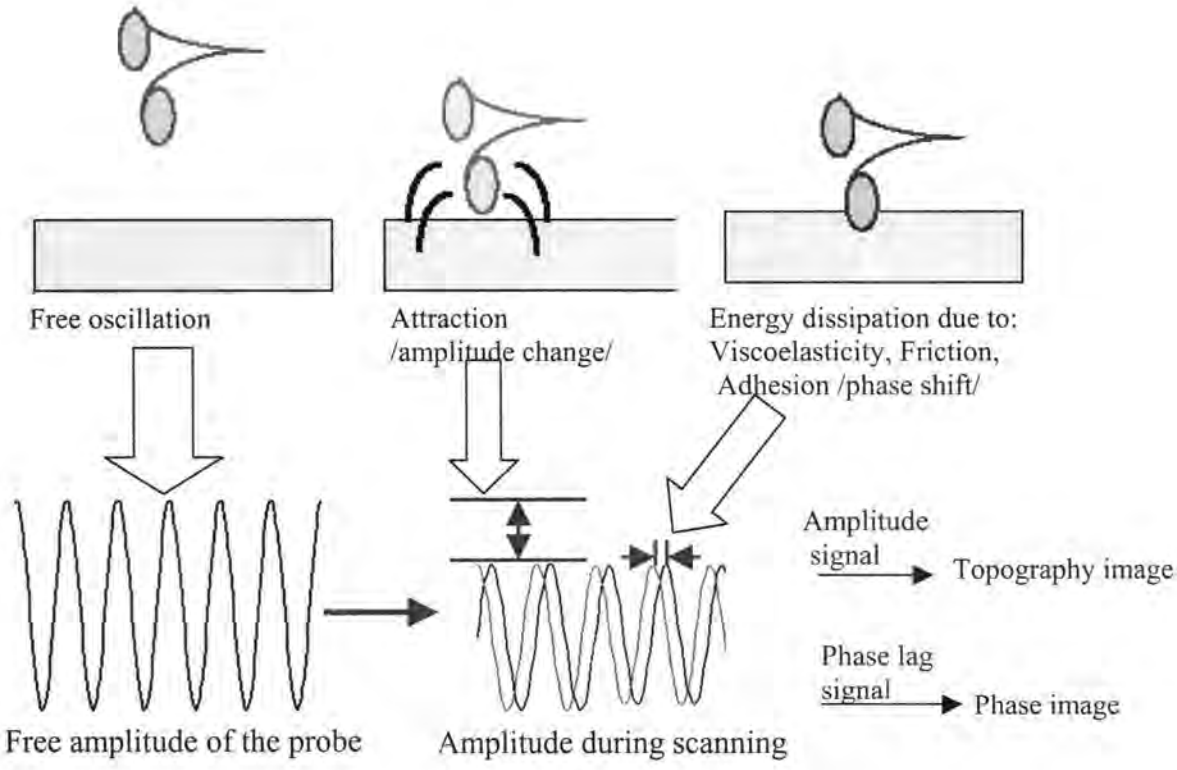

Figure 15. Schematic of tip-sample interactions and image formation in tapping mode AFM.

The capability of direct measurement of 3D surface topography is, probably, the prime advantage of AFM. The resolution of AFM in the z-direction is different from that in the X-Y directions. In the Z-direction (perpendicular to the sample surface), the resolution of AFM primarily depends on the sensitivity of the cantilever and the z-piezo and it is in the order of 0.1 nm, and, in most cases, it is considered sufficient.

The lateral resolution of an AFM image is determined by the geometrical convolution of the tip and the sample (Figure 16). Therefore, some precautions have to be taken when working with very small objects, like protein single molecules. To avoid deformation of the sample with the tip, it is necessary to minimize forces during scanning, applying so-called 'light' tapping.[58] In addition, knowledge of the tip radius is required to measure lateral dimensions of an object.

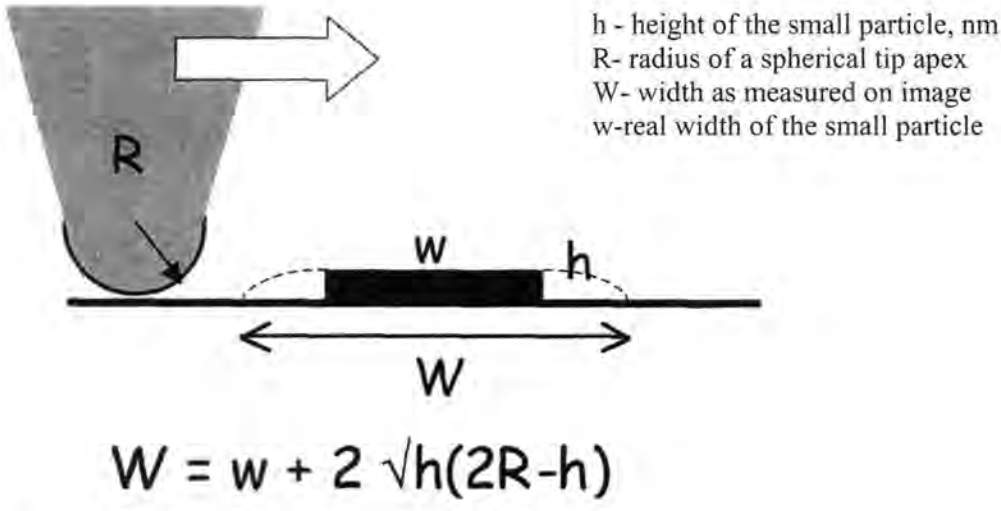

Figure 16. The effects of tip broadening of small objects

Tip radius can be measured independently by scanning gold nanoparticles.[59] This technique is based on several assumptions: 1) gold nanoparticles have spherical shape, and 2) error in height measurement is negligible. This way, the measured height and apparent width of the nanoparticle allow estimating the tip radius as it is shown on Figure 17.[59]

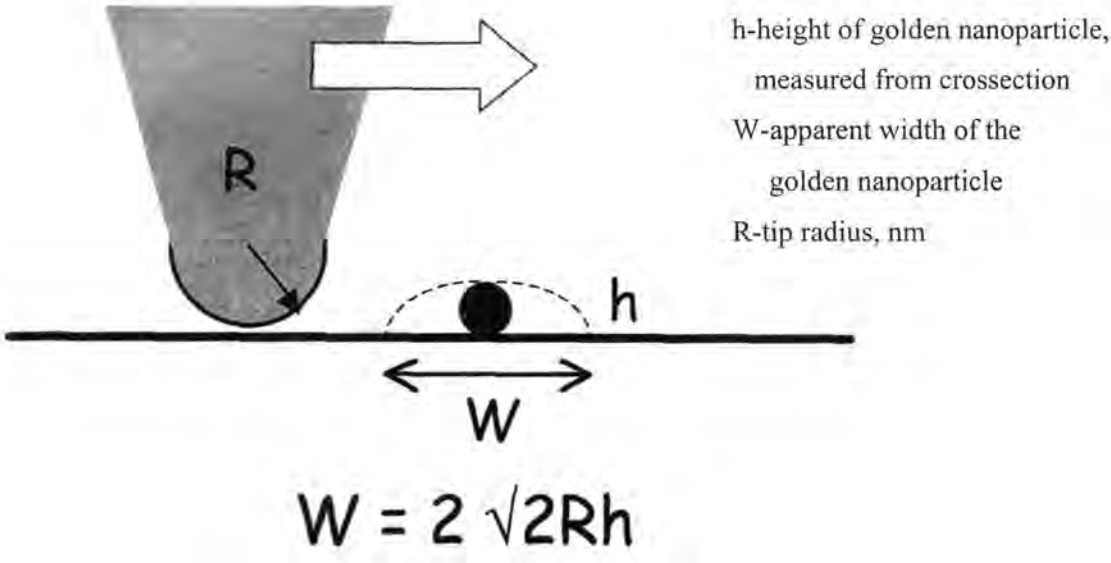

Figure 17. Estimation of the tip radius.

In this research, AFM study of the deposited LB layers and the SAM layers is performed on both Dimension-3000 and Multimode microscopes (Digital Instruments) in tapping mode.[60,61] Scanning is conducted at 1 Hz scanning rate, for scales ranging from 30x30 μm down to 300x300 nm, and for several randomly selected surface areas. Typical AFM tip radius range is between 10 and 30 nm and typical spring constants are from 40 to 60 N/m.

4.4.2. Ellipsometry

Ellipsometry is a sensitive optical technique for determining the thickness of thin films. When linearly polarized light of a known orientation is reflected at oblique incidence from a surface then the reflected light is elliptically polarized. [62] The shape and orientation of the ellipse allows the thickness of the layer to be calculated.

We measure film thickness using a COMPEL Automatic Ellipsometer from InOmTech, Inc. with an incident angle of 70°. The silicon oxide layer is measured after wafers are cleaned with piranha solution. The average thickness is found to be between 0.9 and 1.3 nm for different wafers. The thickness of the deposited layers is measured taking into account the oxide layer. The indices of refraction used for the layers are 1.45 for ODTMS, 1.55 for OTS, and 1.45 for lipid-protein mixtures.[52] An averaging over five measurements from different location on the substrates is performed.

4.4.3. Contact angle

Measurement of contact angles with other surface characterizing techniques can give information about the chemical structure of the surface and its influence on the surface energetics. The contact angle of a liquid droplet resting on a surface at equilibrium is described by Young equation:[63]

$$\gamma_{LV}\cos(\theta) = \gamma_{SV} - \gamma_{SL} \quad , (2)$$

where γ_{LV} is the surface tension of the liquid in equilibrium with its saturated vapor, γ_{SV} is the surface tension of the solid in equilibrium with its saturated vapor of the liquid, γ_{SL} is the interfacial tension between the solid and the liquid, and θ is the contact angle.

Figure 18. Example of contact angle measurement.

The contact angle is measured using a sessile drop technique on a custom-made stage equipped with a digital microscope (Intel Play Qx3). The micropipette is filled with NanoPure water and droplets of 5µl are placed on the sample's surface. The angle between the water droplet and the surface is measured on the monitor using a protractor (Figure 18). Reported contact angle values are averaged over five measurements taken at different locations on the sample.

4.4.4. Molecular modeling

Molecular imaging software allows visualization of biological macromolecules. A created 3D image can be displayed at any angle; dimensions of the protein can be measured. Molecular models are created using Rasmol software and the protein structure data files from ProteinDataBase. [64]

CHAPTER 5. RESULTS AND DISCUSSION

5.1. Adsorption of Hemolysin onto a bare silicon

Here, we study adsorption of Staphylococcal α-Hemolysin from aqueous solution onto a bare silicon substrate. The topography image shows a close packed layer of spherical particles (Figure 19). The dark color of the background in the intervals between molecules corresponds to the silicon surface.

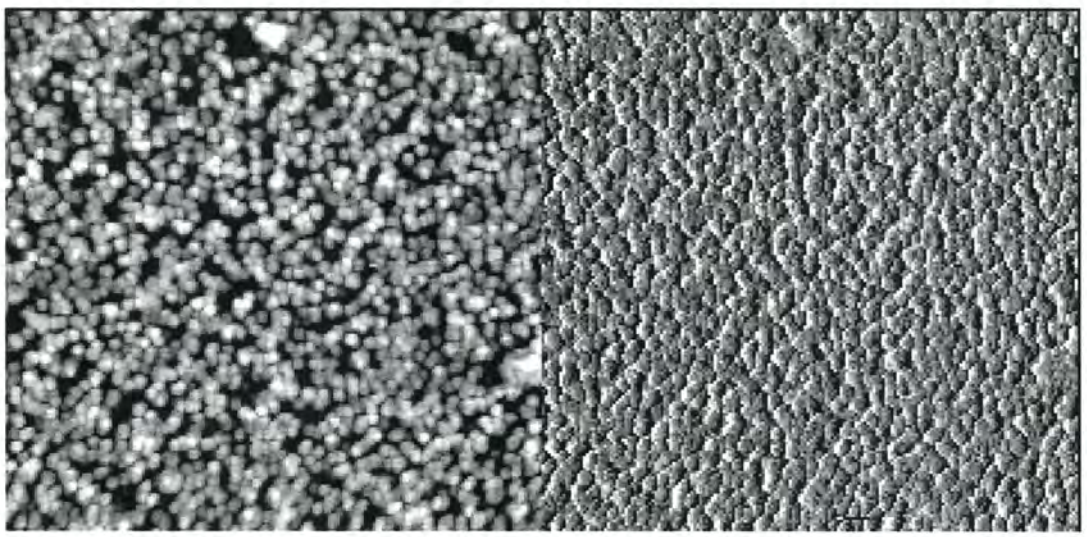

Figure 19. 1×1 μm AFM tapping mode image (topography- left, phase-right) of α-Hemolysin after absorption on the bare silicon. Topography image Z range is 5 nm, phase image Z range is 80 deg.

The surface morphology in the phase image appears different from the topography image. In the phase image, particles appear larger and merged together. The phase mode contains information about tip-sample interactions, especially adhesion forces (see Fig. 15).[65]

In this experiment, the sample is dried for a short time only to assure minimum damage of the protein due to dehydration. Even though the sample is visually dry, it contains molecular surface layers of water. This water gives rise to the capillary forces between the AFM tip and the sample surface, which cause damping of the tip oscillation (Figure 20), and as a result, the protein molecules appear larger than on the phase image on topography.

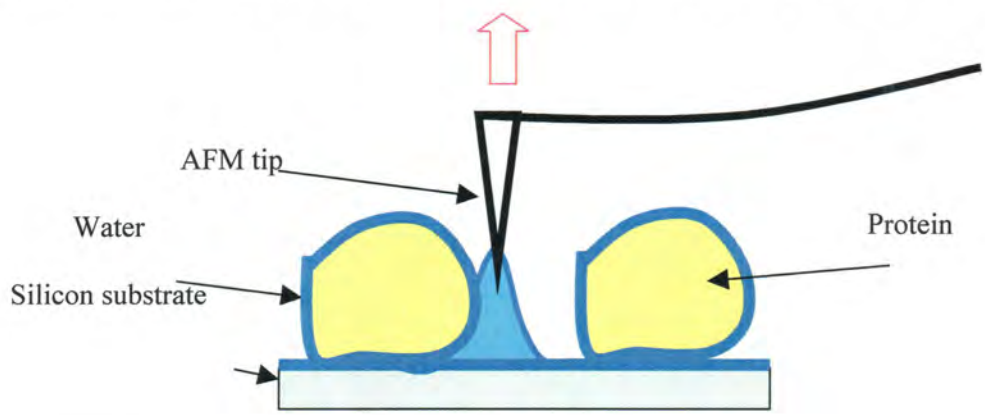

Figure 20. Schematic of capillary effect on the phase image.

Adsorption of the protein from diluted solution results in a few single spherical particles observed in a 1×1 μm surface area (Figure 21). The protein molecules are located further apart than after adsorption from solution with higher protein concentration. The molecular conformation of the protein could be analyzed from topography images of individual molecules.

Actual lateral dimensions of protein molecules are estimated, taking into account the tip radius after the width and height of the molecules are measured on crossections as it was described previously (see Figs. 16, 17). An average height of the protein molecules is 2.1 nm as measured from crossections of individual molecules (Figure 22). The calculated diameter

of the protein molecules is 22 nm, which is more than it is expected. The X-ray crystallography data suggest that the diameter of the hemolysin molecule is 10 nm and the height is 10 nm (Fig. 8).

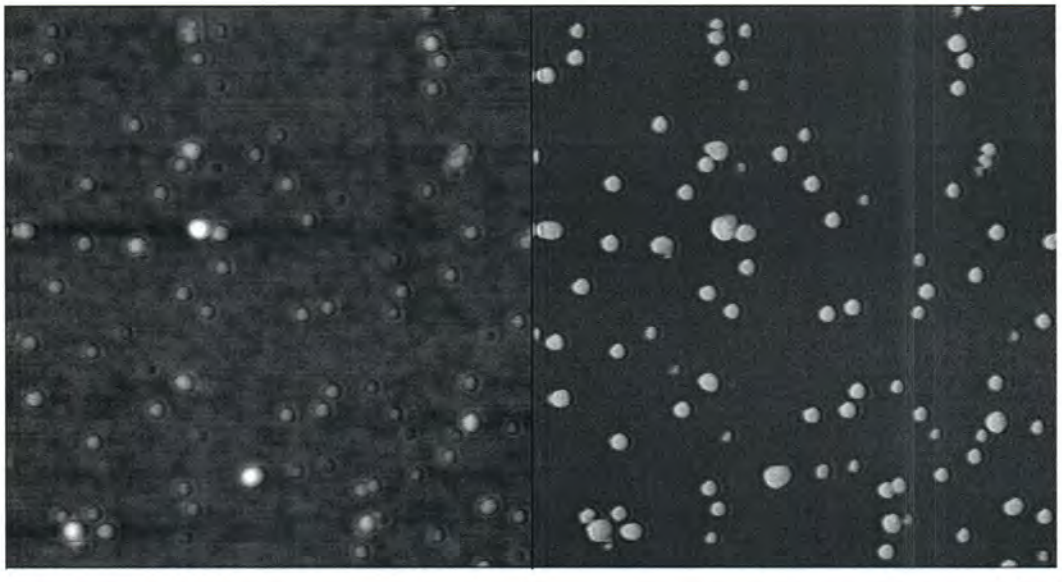

Figure 21. 1×1 μm AFM tapping mode image (topography- left, phase-right) of diluted α-Hemolysin solution on bare silicon. Topography image Z range is 5 nm, phase image Z range is 50 deg.

The diameter of the protein molecules appear much larger than that expected from molecular model. However, the height is significantly less than it should be. Dimensions of the protein indicate that the molecules are collapsed. There are several driving forces for protein deformation, such as protein-substrate interaction and tip-protein interactions. The apparent lowering of heights of the molecules can be the result of compression with the tip, and also it can be a result of adherence of the tip to the protein molecule during scanning (see Fig. 20).

Figure 22. Crossection of an individual hemolysin molecule after adsorbtion onto the silicon.

Flattening of the protein molecule can also be an effect of protein adsorption onto the surface. Observing the chemical composition of the hemolysin molecule helps to understand protein-substrate and protein-tip interactions. Molecular viewer software allows analyzing the distribution of amino acids in the hemolysin molecule. The top part of the Hemolysin has a significant quantity of lysine and arginine side groups on the surface as shown on the molecular model image in Figure 23.

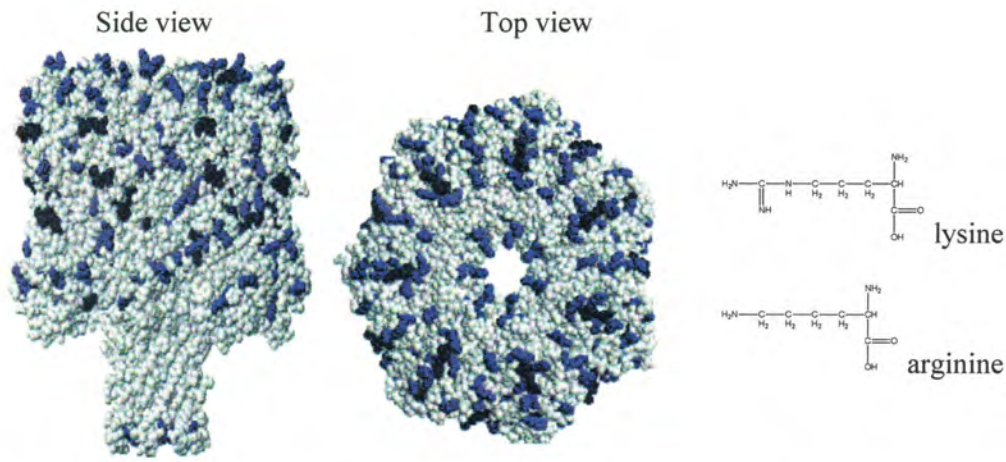

Figure 23. Location of lysine and arginine in α-Hemolysin are shaded, all other amino acids are in gray.

Lysine and arginine expose positively charged end groups at the protein surface. As a result, the hydrophilic part of hemolysin has an overall positive charge on the surface. At the same time, the surface of freshly grown silicon oxide has high surface density of OH groups. In water, silicon oxide is known to have significant negative charge at intermediate pH. Therefore, Hemolysin can have strong bonding to the silicon substrate. Because of this interaction the protein adsorbs in a compact fashion and does not unfold but flatten. [66]

5.2. Adsorption of MscL onto the bare silicon

Behavior of the MscL during adsorption onto bare silicon surface is different from Hemolysin. Unlike α-Hemolysin, MscL tends to form agglomerates. AFM image of MscL after adsorption onto the silicon substrate are presented in Figure 24.

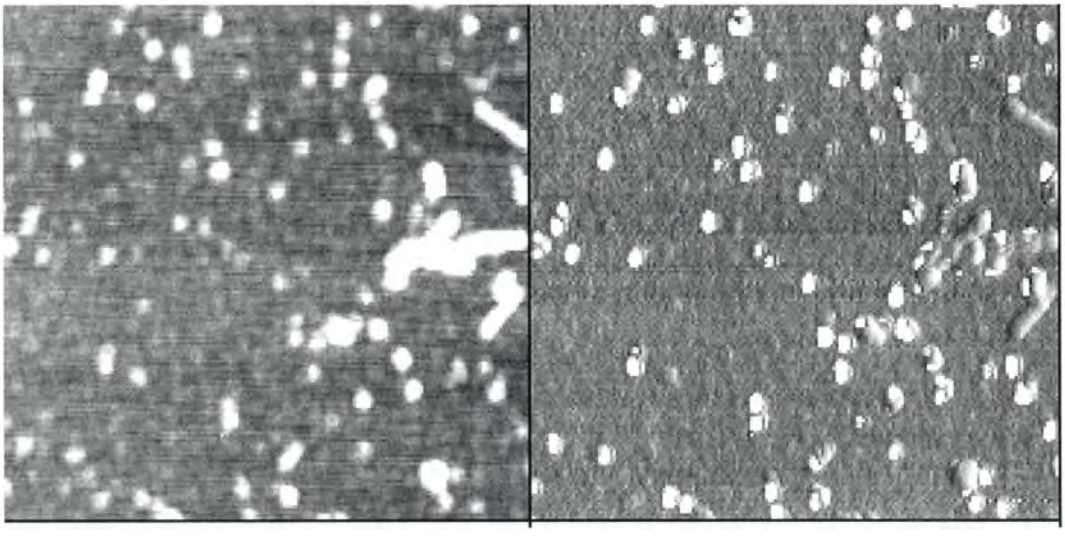

Figure 24. 1×1 μm AFM tapping mode image (topography left, phase right) of MscL after absorption on bare silicon. Topography image Z range is 5 nm, phase image Z range is 15 deg.

The image obtained after adsorption of stock solution of the protein (0.36 mg/ml), without dilution shows the presence of round shaped particles, and large agglomerates. Low z-range of phase image (15 deg) and appearance of the background on topography image indicate that the probe is scanning over soft polymer-like thin film on the surface but not bare silicon.

Thus, the substrate is completely covered with unfolded protein. Individual protein molecules in a partially unraveled state are adsorbed on top of this layer. Protein molecules also occasionally form aggregates on the surface (Figure 25).

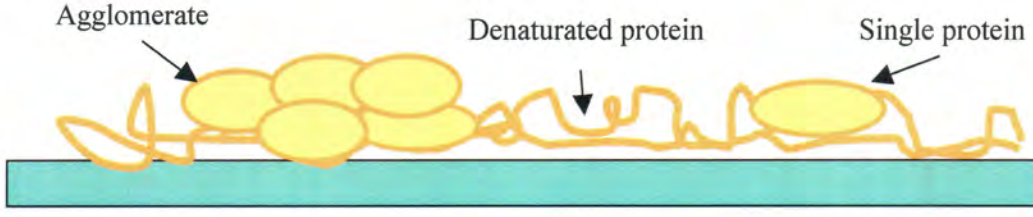

Figure 25. Sketch of MscL layer adsorbed on the bare silicon.

Analysis of the protein composition allows addressing the nature of interactions with the substrate. First off all, unlike hemolysin, MscL forms agglomerates during adsorption onto silicon surface As it is clear from molecular models, MscL has an almost completely hydrophobic surface. Figure 26 shows contrast in distribution of hydrophobic and hydrophilic amino acids in molecular structures of the two proteins. The surface of the MscL molecule is much more hydrophobic compare to hemolysin, therefore it has tendency to

aggregate. It is known that membrane proteins tend to form agglomerates in aqueous solutions because of their primarily hydrophobic nature.[67]

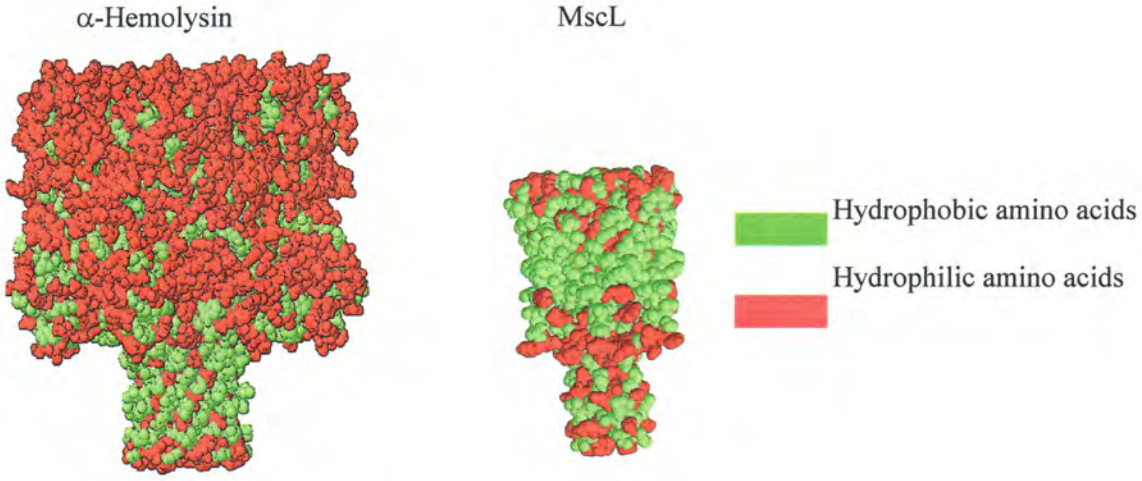

Figure 26. Distribution of hydrophilic and hydrophobic aminoacids in α-Hemolysin and MscL.

MscL is also probably completely unfolded on the silicon substrate surface. MscL during adsorption on silicon unfolds in order to expose hydrophilic groups to the surface. This conformational change is favored by the lowering of the free energy of the silicon-oxide surface by adsorption of the protein. The thermodynamic barrier between the native state and the unfolded conformation of protein is low, only 21-63 kJ/mol, and the energy of adsorption can much higher.[68] Therefore proteins change conformation in order to adjust to the surface. However the extent of this conformational change is different for hemolysin and MscL.

5.3. LB monolayer of α-Hemolysin

Hemolysin heptamer is a large compact molecule and, in a pure state, it is not soluble in water. However, it can exist in solution when solubilised by surfactants such as SDS.[69] Hemolysin has a highly hydrophilic large top part or cap, and hydrophilic narrow stem (see Fig. 28). Separation of hydrophobic and hydrophilic regions on opposite ends of the molecule provides hemolysin with amphiphilic properties. It is able to form a continuous monolayer at the air-water interface. An AFM image of Hemolysin deposited on silicon as LB monolayer is presented on Figure 27.

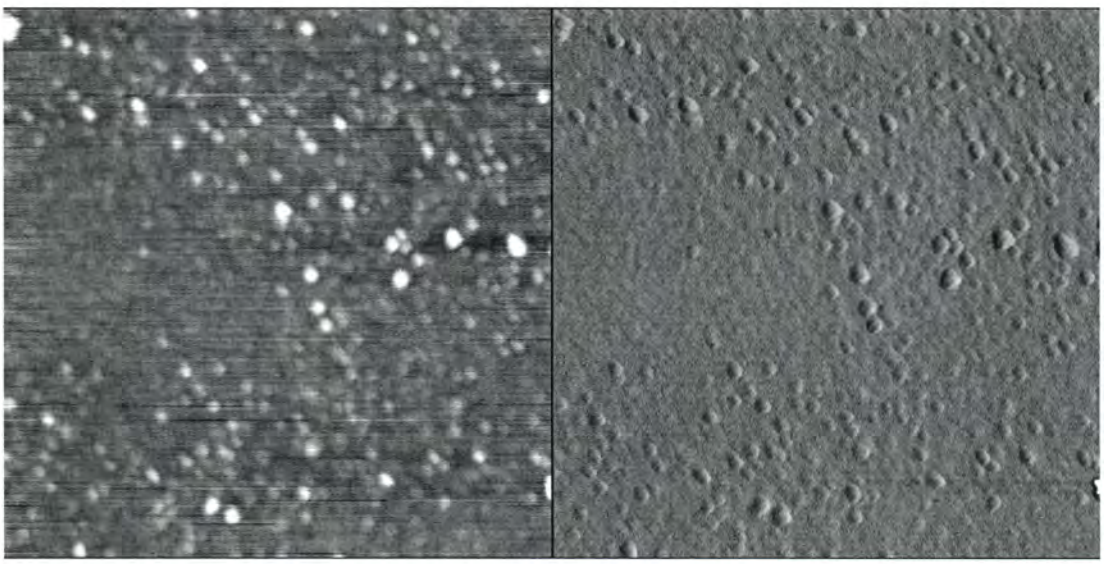

Figure 27. 1×1 μm AFM tapping mode image (topography left, phase right) of LB deposited Hemolysin on bare silicon. Topography image Z range is 5 nm, phase image Z range is 15 deg.

The morphology of the LB monolayer of Hemolysin resembles adsorption of MscL onto bare silicon. Low z range on the phase image indicates that the substrate is completely covered with denaturated protein. Protein molecules appear distorted, if compared to the

AFM image after adsorption of Hemolysin onto bare silicon (see Figures 21, 23). Denaturation of proteins on air-water interface is studied mostly for globular proteins. Radke, using tensiometry and total internal reflection spectroscopy reported dynamics of unraveling of albumin. [70] According to his results, adsorption of proteins at air/water interfaces leads to partial unraveling and denaturing, and formation of a viscous elastic, gel-like surface phase.

5.4. LB deposition lipid monolayers with MscL and hemolysin

Reconstitution of Hemolysin and MscL into a lipid monolayer is performed in several different ways. Hemolysin spontaneously incorporates into the lipid layer on the air-water interface in the Langmuir trough because of its amphiphilic nature. MscL is soluble in water, and our preliminary experiments have shown that this protein has no tendency to collect at the air water interface, unlike hemolysin. Therefore a special routine utilizing the liposome fusion technique was developed for MscL protein reconstitution into the lipid monolayer at the air-water interphase.[55]

Deposition of Hemolysin and MscL on silicon in mixed lipid-protein monolayers seems to prevent both proteins from complete unraveling. AFM images show the presence of individual protein molecules embedded in the lipid monolayer as nanoscale bumps surrounded by uniform lipid surface (Figure 28). Lipid monolayers also prevent formation of agglomerates of proteins. Smooth spherical shapes with diameter 16 nm for MscL and 20 nm for hemolysin are observed for proteins deposited in lipid LB monolayers.

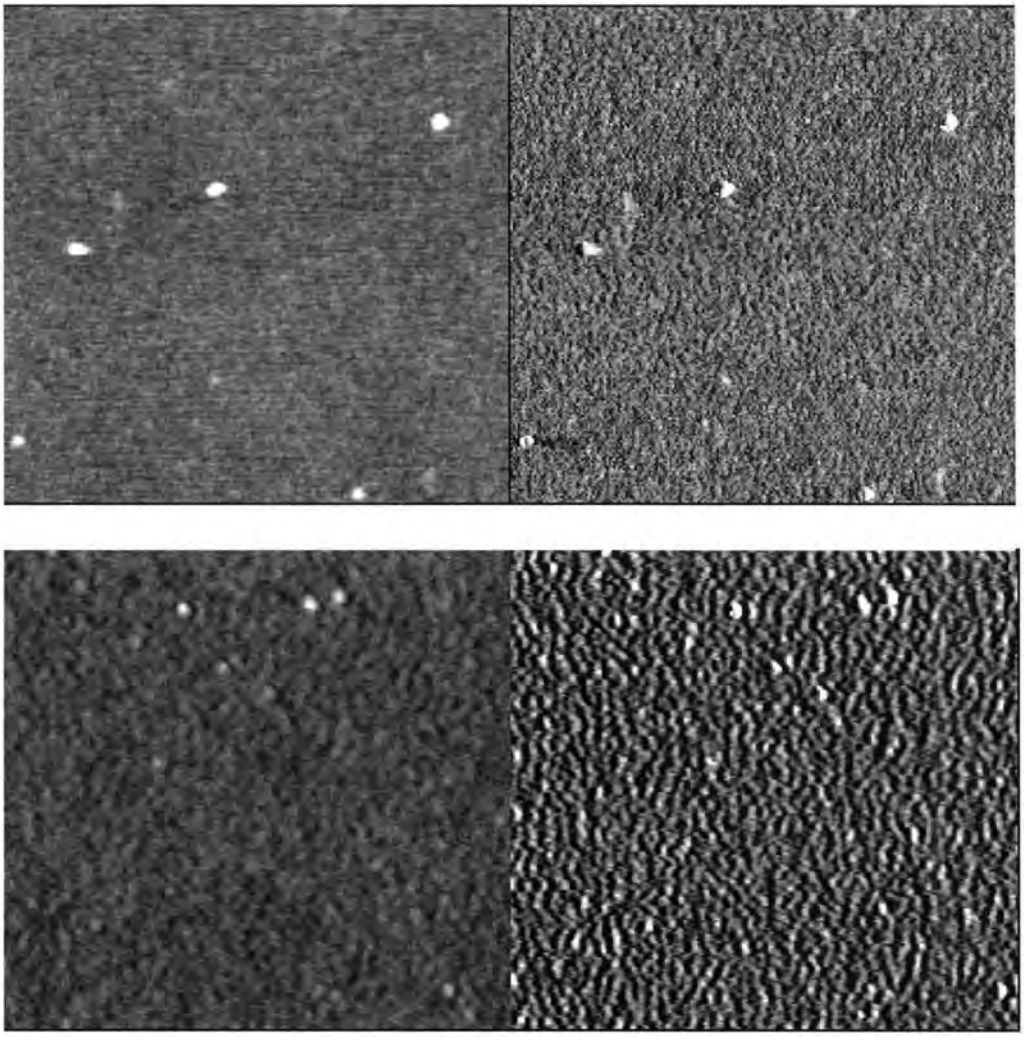

Figure 28. 1×1 μm AFM tapping mode images (topography left, phase right) of LB monolayers of phosphatidylcholine with proteins deposited onto bare silicon. Top: staphylococcal α-toxin, bottom: MscL. Topography image Z range is 5 nm, phase image Z range is 20 deg.

Dimensions of proteins embedded in lipid monolayers are measured according to the model presented in Figure 29. This model calculates the height of protein molecules by adding the thickness of the lipid layer and protein height above the lipid monolayer. The

thickness of lipid monolayers in these experiments is 1.6 nm, as it has been measured separately by ellipsometry.

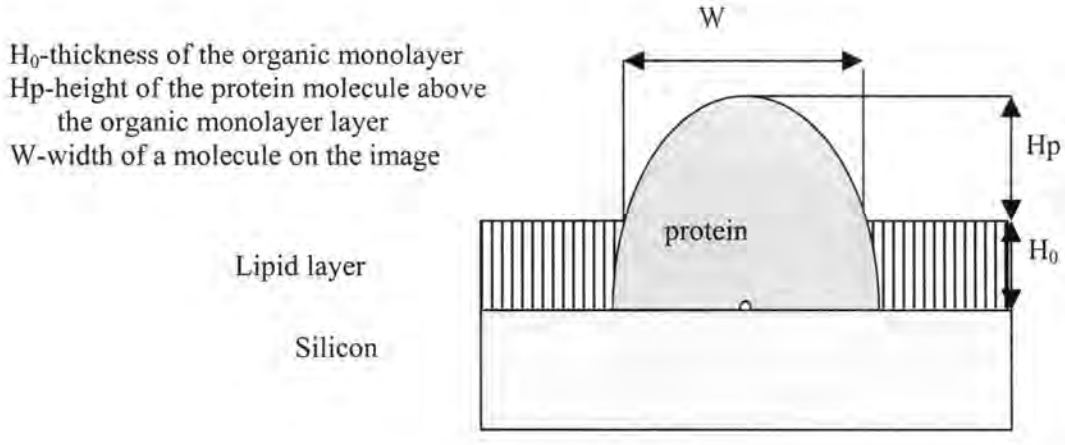

Figure 29. Sketch of protein incorporated into organic monolayer.

The height of individual macromolecules did not exceed 3.4 nm for hemolysin and 2.8 nm for MscL. These values are much lower than expected for the proteins (see Table 1). However, this is significantly higher than measured on the bare silicon. This thickness, along with the absence of any signs of recognizable pore structure indicates collapse of the protein molecules but less deformation compared to the protein deposited directly on the bare silicon surface. The substantial quantity of hydrogen bonds between polypeptide and substrate causes adhesion and spreading of protein globules on the silicon surface. Apparently, addition of organic monolayer results in minimization of protein unfolding due to the reduction of surface tension of the substrate.

5.5. ODTMS SAM fabrication

As it was described previously, substrates with high surface energy tend to disrupt the conformation of the ion channels. ODTMS SAMs are used in this research as a model surface with lower surface energy fro ion channel adsorption. To be able to identify the protein molecules, it is necessity to immobilize molecules on a flat, atomically smooth substrate. As it is known the quality of alkylsilane SAMs is very sensitive to conditions of fabrication. Therefore, special attention in this research is paid to quality of SAMs.

Alkylsilanes react actively with silanol (SiOH) groups on glass or on silica surfaces. It was shown that alkylsilanes react directly with silanol groups on the surface. [71,72] They form an immobilized film of a single layer alkyl chains on the reacted surface (Figure 30).[73] At first stage of SAM formation, alkylsilane molecules adsorb to the highly hydrophilic surface of silicon dioxide. Then the alkylsilane molecules form covalent bonds with available silanol groups on the surface. Resulted SAMs of alkylsilanes are chemically stable.

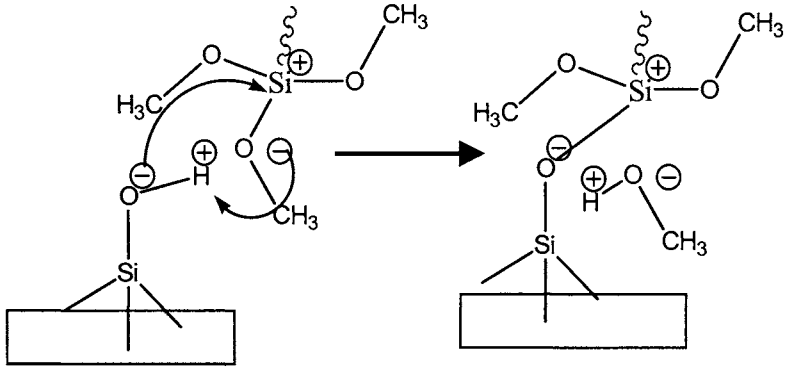

Figure 30. Chart of chemical reaction of an alkyltrimethoxysiloxane with silicon surface.

As known, alkylsilanes are extremely reactive in the presence of water. In anhydrous solvents alkylsilanes form monolayer on the surface, but in presence of water in solvent, silanol groups have a tendency to form agglomerates(Figure 31).[74] The water reacts with the methoxy group to form silanol and free methanol. Silanol groups can effectively initiate dimer with the next molecule, and so forth. Therefore the presence of contaminant water in the solvent induces silane aggregation in solution, resulting in the deposition of particles with heights that are often indistinguishable from proteins.

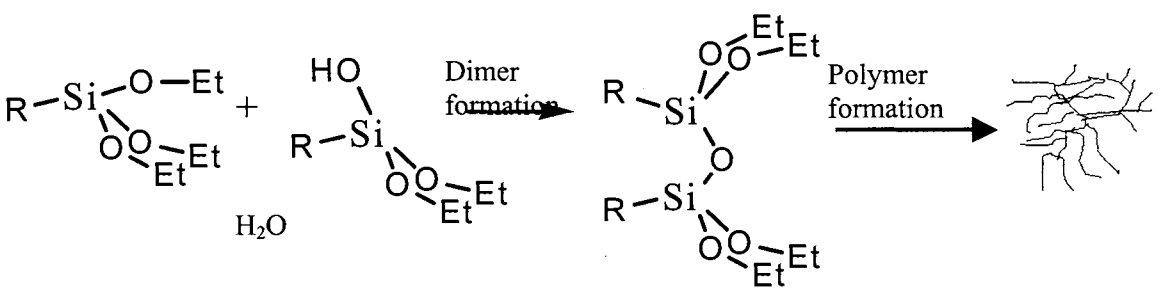

Figure 31. Formation of silane agglomerates in solution. [74]

In this research, ODTMS SAMs on silicon are fabricated using liquid adsorption technique. Surface density of ODTMS SAM is controlled by the interruption of adsorption at different stages. The formation of silane agglomerates on the surface results in higher roughness. To produce smooth uniform surface, silane modification is conducted in dry nitrogen atmosphere in anhydrous solvents. Solvents and ODTMS are distilled before SAM fabrication.

Obtained ODTMS SAMs with various densities of grafting typically show absolutely flat uniform organic layer (Figure 32). Measured AFM roughness of the ODTMS SAMs used for protein immobilization is between 0.3 and 0.6 nm in 1×1 μm surface area.

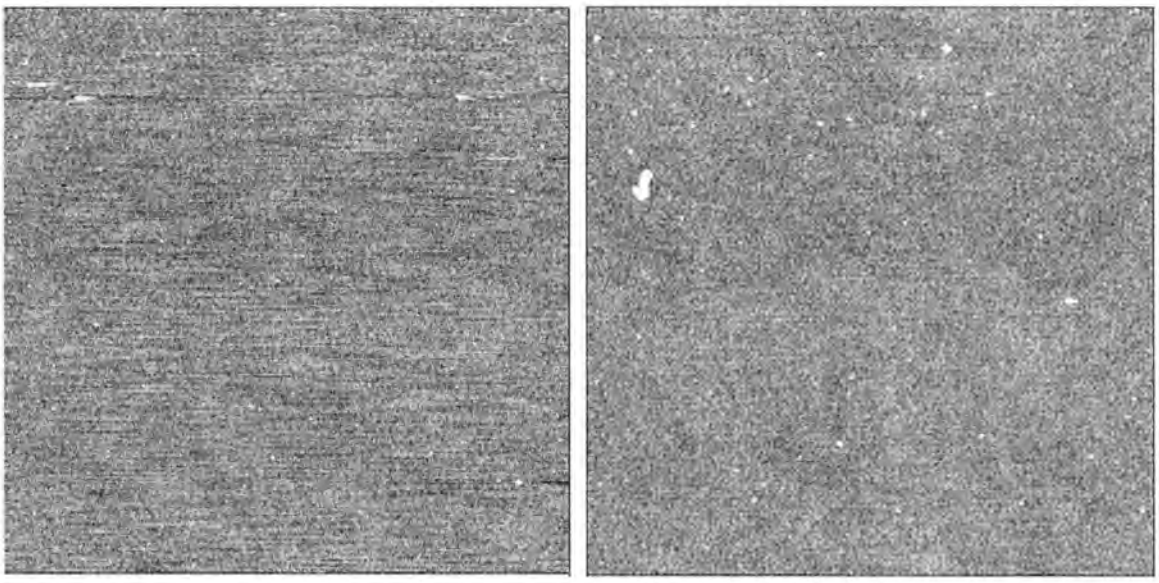

Figure 32. 5×5 μm AFM tapping mode topography images of adsorbed ODTMS monolayer after 20 min (left), and 21 h of adsorption (right). Z range is 5 nm.

Figure 33 presents the contact angles and thickness for SAMs as a function of deposition time within the time range from 10 min to 21 h. The measurements show the typical kinetics of molecular chemisorption from solution observed for alkylsilanes. [75] The thickness rises quickly within first 20 min from close to zero for a clean silicon wafer to 80° and then gradually increases to 104° at 21 hour adsorption.

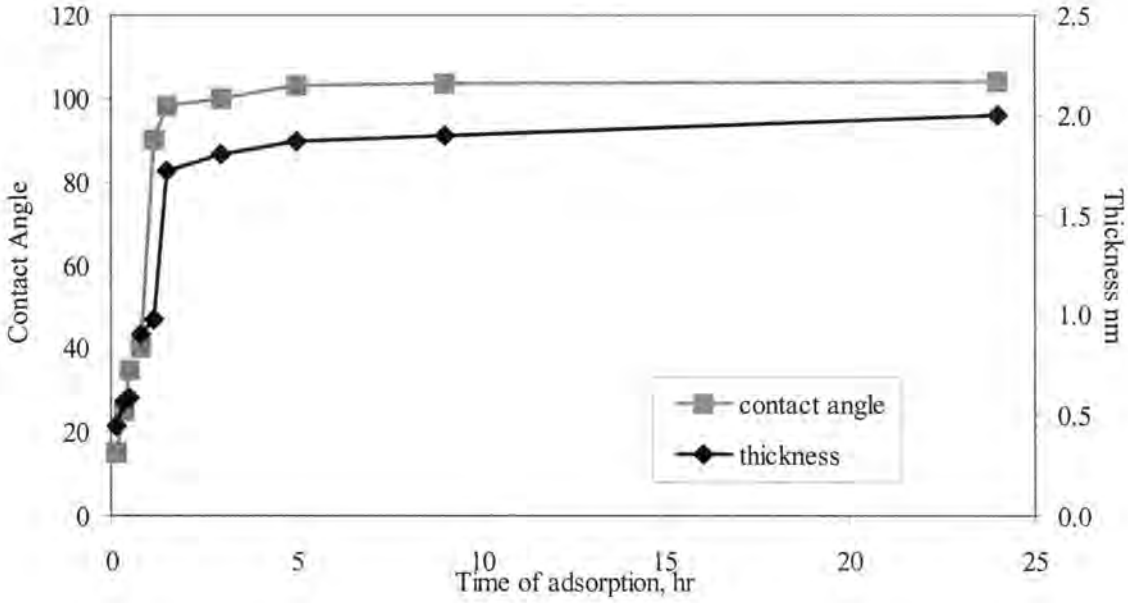

Figure 33. The variation of the thickness of ODTMS SAM with time of adsorption.

The maximum thickness of the adsorbed monolayer of 2.0 nm is smaller than that expected 2.5 nm for fully extended C18 alkyl chain. The density of packing during adsorption of ODTMS from solution is not high enough to reach crystalline packing and stretch alkyl chain. ODTMS molecule has to reach the surface to be able to form a chemical bond because of the bulkiness of the reactive group. First step of adsorption is fast and it is described with diffusion - controlled kinetics.[76] During adsorption process, as the surface area becomes more populated, the free space available for new adsorbing molecules lessen. At that point, the rate of adsorption declines.

Maximum achieved coverage of the surface with alkyl groups, however, is high enough to make the surface highly hydrophobic. Maximum contact angle observed for ODTMS

layers is 100° after 2 hours of adsorption. In literature, the water receding angle of 100-104° is reported for substrates with dense alkyl-silane SAMs.[73] Contact angle shows gradual linear increase with thickness of SAM (Figures 33,34).

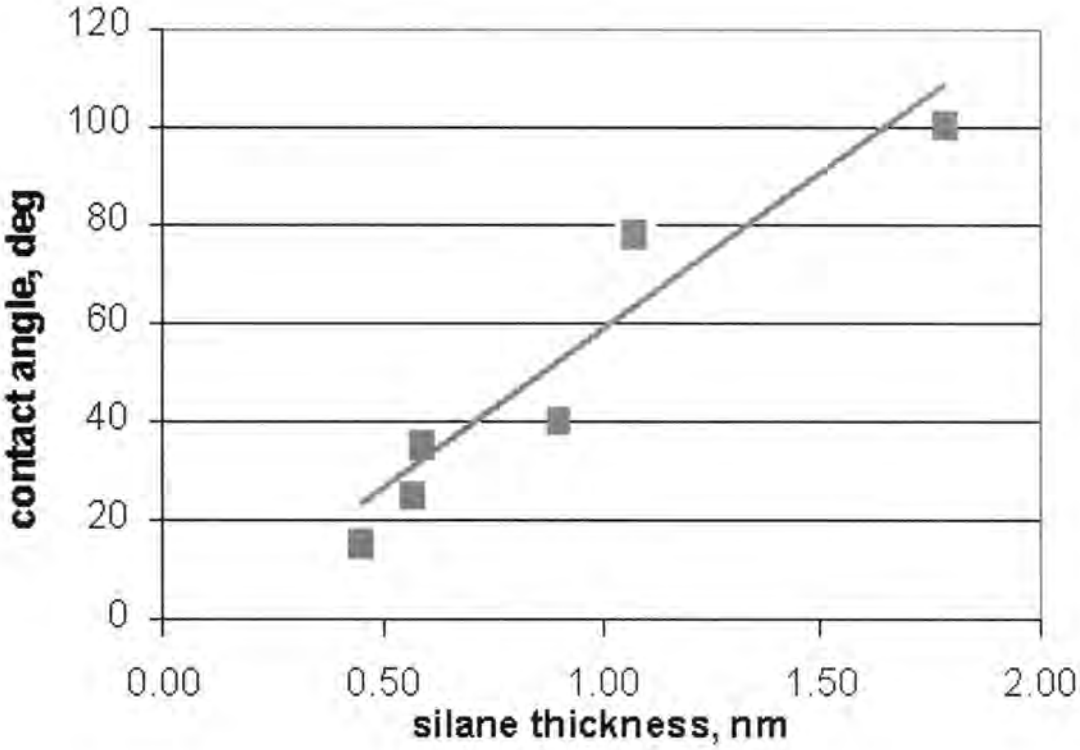

Figure 34. Correlation between ODTMS monolayer thickness and contact angle of water.

Contact angle measurements can be analyzed in terms of 'apparent surface' coverage or the fraction of silicon surface screened by a film. The Cassier equation assumes a simple 'two-phase' model of surface structure and provides the relationship:[77]

$$\cos\Theta_m = \beta\cos\Theta_L + (1-\beta)\cos\Theta_{Si} \qquad (3)$$

where Θ_m is the measured contact angle, Θ_L is the contact angle for the complete layer, and Θ_{Si} is the contact angle of bare silicon. The Cassier equation is based on averaging involving the interfacial free energies of each of the two components and assumes homogeneous coverage.

Interruption of the adsorption process after different times intervals allows producing substrates with different density of grafting (Figure 37). ODTMS SAM demonstrate higher contact angle and therefore have lower surface energy.

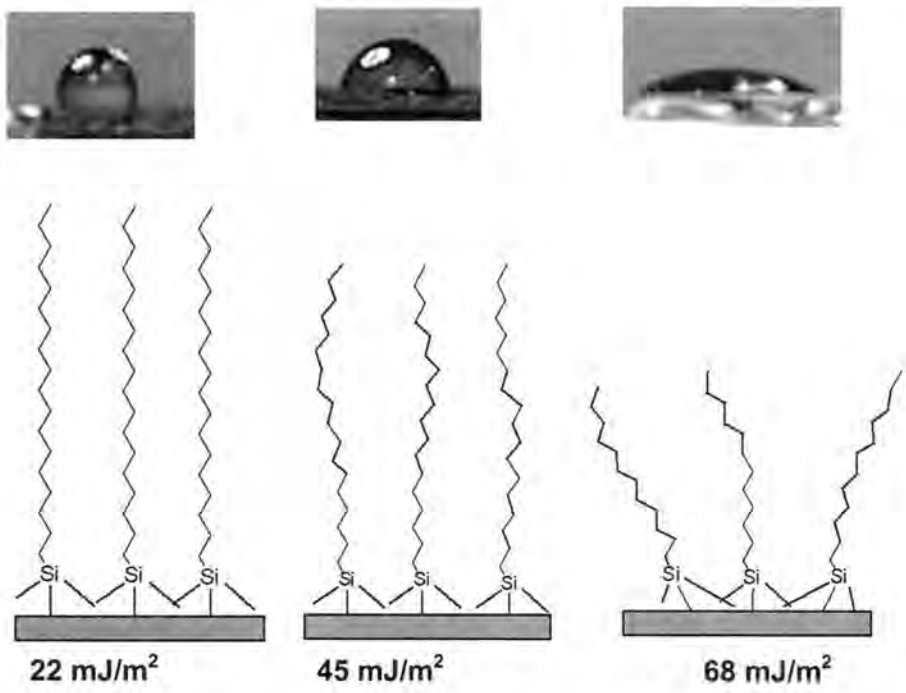

Figure 35. Correlation of alkyl chain packing and surface energy.

5.6. Adsorption of MscL onto homogeneous ODTMS SAM

The three-dimensional structure of a protein in a particular environment is the result of intermolecular interactions and interactions between the protein and the environment. Membrane proteins are stabilized mostly by hydrophobic interactions. Therefore alkyl region of lipid membrane is a crucial component for structure stabilizing. It was demonstrated before, how alkylthiol SAMs of different density incorporated gramicidin, a low molecular weight ion channel, in different orientations.[78] In this chapter we describe the adsorption of MscL onto a variety of well-characterized alkyl modified surfaces.

Incomplete layers of ODTMS adsorb MscL. Figure 36 gives representative images of ODTMS substrates after protein adsorption. Adsorption onto loosely packed SAMs with estimated surface tension 45 mJ/m^2 resulted in the formation of compact, globular particles 2 nm height about and about 10 nm diameter. Pore structures are not apparent. Surface concentration of adsorbed protein is very low, about 3-5 molecules per 1 μm^2.

Very different structure was observed for proteins adsorbed on low density SAMs. The estimated surface energy of SAM after 20-minute adsorption is about 68 mJ/m^2, which is just little lower than surface energy of a bare silicon substrate (72 mJ/m^2).[77] Significant number of well-defined, donate-like shape particles of adsorbed protein molecules is observed. Height of the protein above SAM is 1.4 nm. The thickness of the SAM is 1.2 nm, therefore maximum height of the protein structure is 2.6 nm, if we assume that protein molecule penetrates full depth of the SAM (see model Fig. 29).

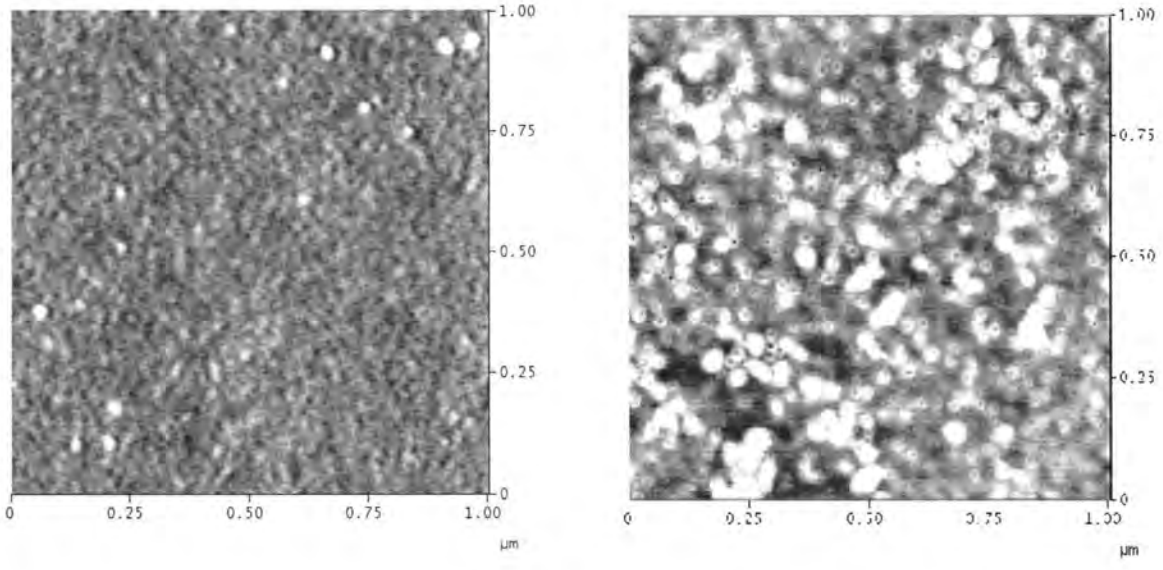

Figure 36. AFM topography images of MscL adsorbed onto ODTMA SAM of high density (left) and low density (right).

Finally, MscL does not adsorb at all on saturated ODTMS. No molecules are observed on AFM scans. Estimated from contact angle surface energy of the saturated ODTMS SAM (highest density) is about 25 mJ/m^2, which is in good correlation with surface energy of dense alkyl-SAM. [77] Both the protein and the substrate have low surface energy, therefore the adsorption of protein does not occur.

AFM images of MscL show clear different structures of the protein adsorbed on different SAMs. Differences in structure of reconstituted MscL are associated with density of SAMs. In loose SAM, MscL is lower and wider than in dense SAM. Moreover, the channel

opening could be seen on AFM of MscL only in loose SAM. Summary of protein conformations on different SAMs is given in Table 2.

Table 2. Summary chart of MscL adsorption onto ODTMS.

Supporting layer	Contact angle, deg	SAM thickness, nm	Protein height, nm	Protein width, nm
ODTMS, saturated	100	2.0	No adsorption	No adsorption
ODTMS, medium	60	1.6	4.5	6
ODTMS, loose	30	1.2	2.6	13

5.7. ODTMS pattern

Several studies reported effectiveness of patterned supporting SAMs for stabilization of lipid layers due to enhancing contact area of lipid layer and solid supports. [79] In our attempt to utilize this approach, a mixture of two surfactants, PFTDA and ODTMS, is used to create pattern on the silicon (Fig. 10). Spontaneous phase separation of in Langmuir monolayer, results in the formation of the pattern shown on Figure 37. This is caused by the difference in chemical structures of the surfactants. Presented example of SAM pattern was obtained via LB deposition of mixed monolayer of ODTMS and PFTDA in 3:1 ratio formed at the air-water interface. The surface pattern is represented by a number of bowed grooves and isolated pits within ODTMS SAM. Darker regions correspond to bare silicon exposed after removal of PFTDA component. Light areas represent SAM-screened silicon surface. The cross-section of the topography image shows SAM height close to 2.0 nm. This value is close

the thickness of densely packed ODTMS SAM obtained via adsorption from solution (section 4.4). The lateral sizes of opened silicon patches are about 200-500 nm.

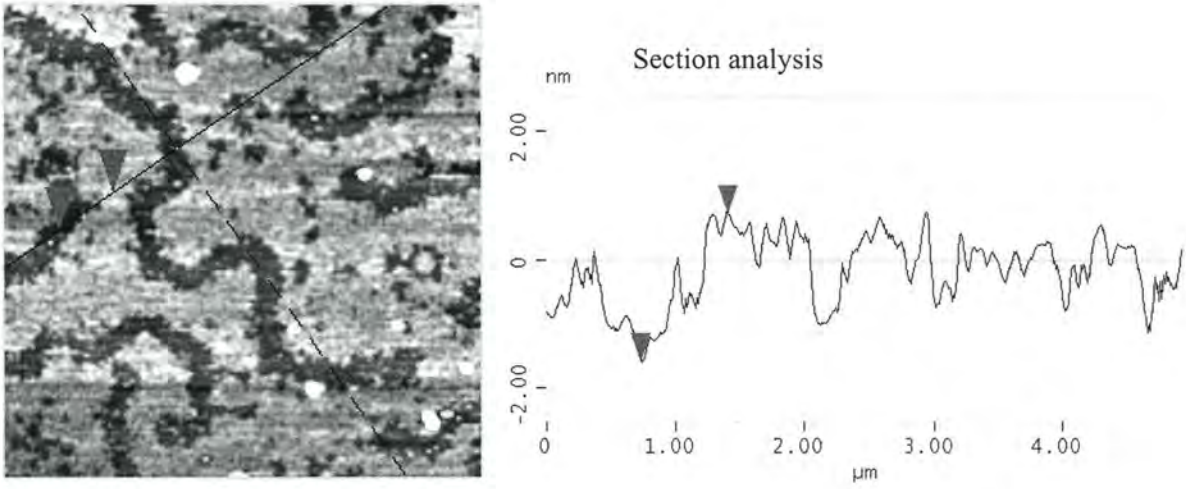

Figure 37. AFM topography image (5×5µm) of ODTMS pattern (left) and corresponding crossection (right). Topography image Z range is 5 nm.

Such a pattern is suitable for high-resolution AFM studies of adsorbed proteins. It provides alternating hydrophilic areas of exposed silicon and areas of smooth, densely packed hydrophobic SAM. Especially attractive feature of this patterned surface is sub-micron dimensions of the hydrophilic surface areas. This allows easy capturing and discriminating of distinct components of a patterned sample on a micron-sized AFM scan.

5.8. MscL in lipid monolayer on patterned surface

Here, liposome fusion is used to assure intact structure of the MscL during adsorption onto solid substrate. Protein-liposome mixture, prepared as described in experimental part, is adsorbed for 1 hour at 4°C on the patterned surface. The excess liquid is quickly removed

from the sample by blowing with a steam of nitrogen for 30 sec. Figure 38 shows AFM image of MscL, reconstituted into lipid phase on the patterned substrate.

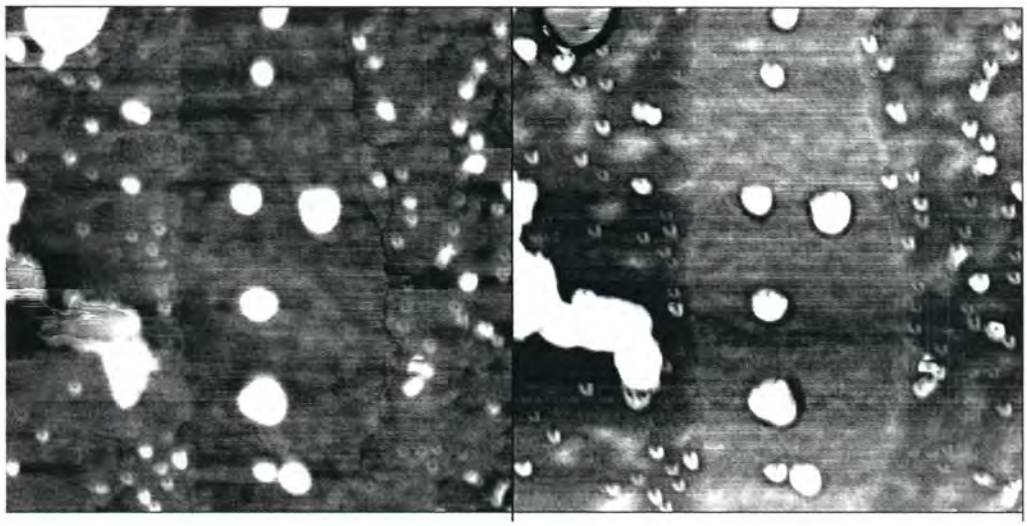

Figure 38. 3.3×3.3 μm AFM tapping mode image (topography- left, phase-right) of MscL reconstituted in lipid on ODTMS patterned sample.Topography image Z range is 5 nm, phase image Z range is 20 deg.

This image shows areas with two different morphologies in the middle and on the sides of the image. In the middle, a vertical line of about 600 nm width corresponds to SAM area. This middle region contains several large, spherical particles on the top of a uniform background. The areas along the right and the left edges correspond to bare silicon areas. Lipid layer patches, composed of phosphatidylcholine-cholesterol mixture, cover these areas. The phase image of the lipid region displays fine marble-like morphology, caused by phase separation in lipid SAM. [80] The central surface area is homogeneous in the phase image. A few small round or V-shaped particles represent single MscL molecules imbedded into lipid.

The crossections of the topography image show no height difference on the border of SAM and lipid–covered areas. The thickness of the SAM pattern before adsorption of liposomes was about 2 nm (Fig.37). The main component of the lipid is egg phosphatidyl choline. This natural lipid is a mixture of phosphatidyl cholines with similar chemical structure of the polar group but different alkyl components. However, the majority of alkyl groups are composed 18 and 16 carbon atoms. Hydrophobic part of lipid is almost the same length with the alkyl group of ODTMS. Therefore, we assume that lipid phase has formed a monolayer on the silicon surface pattern.

There are several larger bumps on the image. The height of these patches above the SAM surface is about 2 nm, which indicates that these are bilayer lipid patches remained on the surface after removal of liposome solution.[81] Considering these results, the mechanism of reconstitution of the MscL could be suggested (Figure 39).

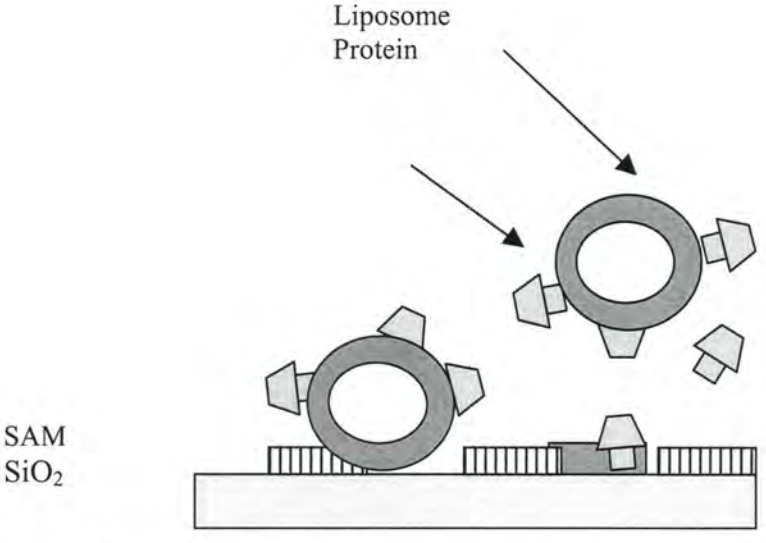

Figure 39. Diagram of liposome fusion with ODTMS patterned.

In this model, lipid vesicles incorporating MscL and adsorb directly on bare silicon of the patterned surface. In fact, the individual MscL molecules imbedded in lipid monolayer could be seen on the high-resolution AFM image (Figure 40). MscL molecules appear as donut-shaped particles about 20 nm across. These shapes resemble an open-pore structure of membrane proteins with a widely open central pore and an elevated ridge.[82]

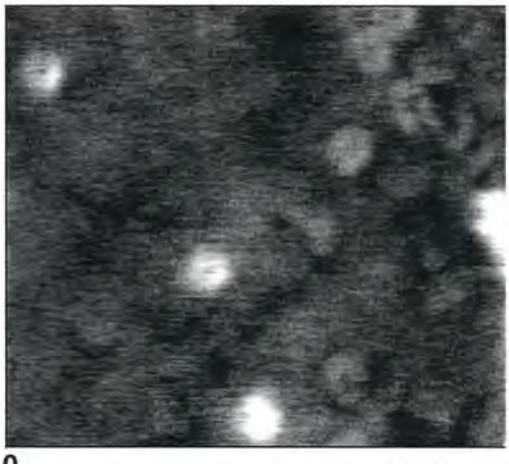

Figure 40. High resolution AFM topography image of MscL embedded in lipid monolayer on patterned surface.

Protein rims are 0.5 nm above the surface as it can be seen from the crossections (Figure 41). The thickness of the SAM as measured independently is 2.0 nm. We assume that molecules penetrate the monolayer on full depth. Thus the estimated height of the embedded protein is about 2.5 nm as calculated according to the model in Fig. 30. The average width of the protein molecule calculated as distance between the rim edges across the molecule is about 13 nm (Figure 41).

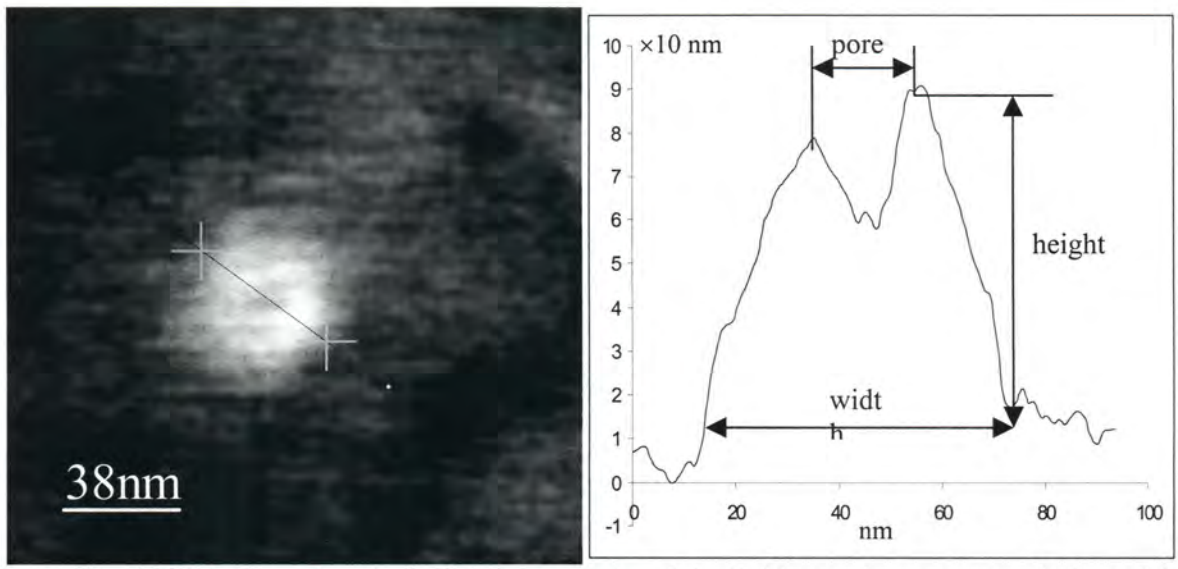

Figure 41. AFM image of a single MscL reconstituted in lipid monolayer pattern (left) and its crossection (right) .

The width of the MscL in opened conformation of the channel should be about 10 nm as predicted by molecular modeling studies. According to this model, in opened state, the height of the MscL is expected to be one-half of the initial channel. However, the difference could be explained by compressing-effect of the AFM tip.[65]

A question about the orientation of protein molecules within the lipid layer could be addressed this way. AFM image gives us evidence that lipid patch is a monolayer. Lipids such as phosphatidylcholine will adsorb on silicon with polar head oriented towards the silicon surface. Cytoplasmic C-terminal region of MscL (smaller barrel) forms total 60 hydrogen bonds with lipid polar groups.[37] During adsorption, these hydrogen bonds could control the orientation of the protein. It means that channel within SAM will be oriented wide rim up, favored by attached lipid molecules.

5.9. Effect of the surface energy on protein immobilization

Functioning of membrane proteins is connected to the lipid-water interface, unlike the globular proteins, which normally exist in a polar aqueous environment. Therefore, the tertiary and the quarterly structure of these membrane proteins is determined to the large extend by hydrophobic interactions with the adjacent matrix. Both α-hemolysin and MscL proteins are anchored within membrane due to hydrophobic interactions between the outer surfaces of the proteins and the inner hydrophobic vicinity of the lipid bilayer. Both proteins form water-filled channels responsible for the permeation of ions across the lipid bilayer.

Models of protein surface behavior revealed in this work are summerized in Fig. 42. Surface adsorption of proteins is favored by lowering free energy of the system.[77] Compliant protein molecule is capable to reduce the free energy of the surface by the price of changing conformation. However, this adjustment could mean disruption of molecular functioning of the protein. The surface of the MscL molecule is almost completely hydrophobic. On the other hand, α-Hemolysin has mainly hydrophilic surface with positive charges. Immobilization of α-hemolysin and MscL in lipid monolayer allows reducing of adherence of hemolysin and preventing of unfolding of MscL on the silicon. It means that interaction with hydrophobic component of lipid is energetically more favored than unfolding of the membrane protein. MscL is more prone to these conformational changes because it is more loosely packed than Hemolysin.

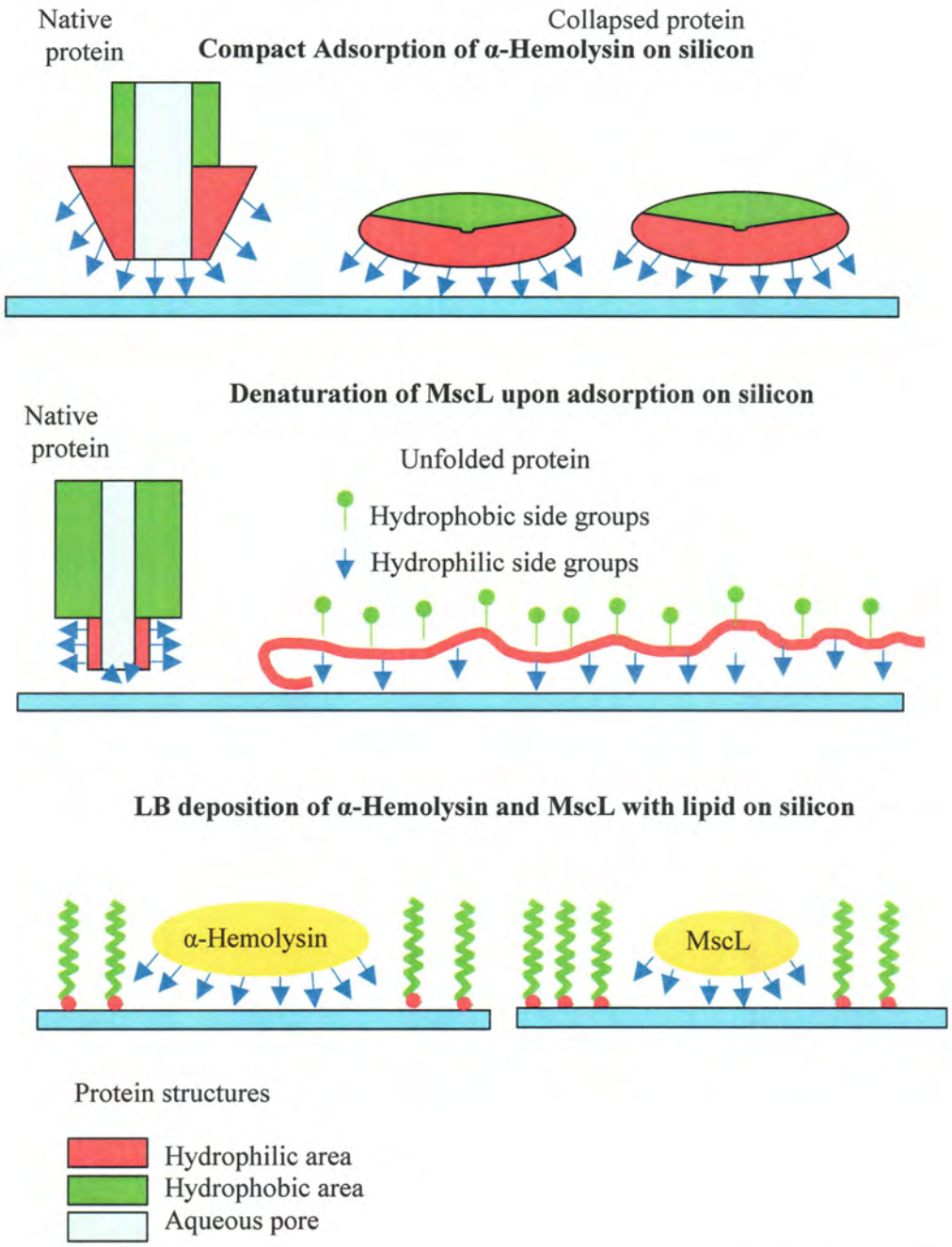

Figure 42. Schematic of effect of silicon surface on conformation of hemolysin and MscL proteins.

MscL, unlike hemolysin, is in closed state in normal conditions. Its state could be regulated by tension in lipid membrane. α-Hemolysin, on the contrary, forms an open pore in the membrane. Our data support the theory that MscL open-closed state is controlled by tension of the lipid layer. The experimental model system includes lipid pattern and ODTMS SAMs on single crystal silicon and homogeneous ODTMS SAMs with different grafting densities. We present existing correlation of molecular models and AFM 3D representations of single MscL molecules in Figure 43A.

From known literature values of surface energies of ethyl groups (20 mJ/m^2) and silicon dioxide surface (72 mJ/m^2) and measured contact angles, we estimated effective surface energy (tension) of modified surfaces ranging from 22 mJ/m^2 for hydrophobic monolayers to 68 mJ/m^2 for loose disordered monolayers (see water drop behavior in inserts in 43A). [83] Initial studies showed that proteins could not tethered or embedded on highly hydrophobic surface with surface tension below 22 mJ/m^2. On the other hand, surface tension exceeding 68 mJ/m^2 results in complete unfolding of protein molecules and their spreading over the hydrophilic surface because of excessive interfacial tension. For intermediate interfacial tensions, we observed a spectrum of protein states ranging from closed state to a widely open state.

Our observations of distinct different shapes of the MscL molecules immobilized in different organic monolayers can be understood considering different conformational states proposed before (Fig. 43B,C).[1,2,10,16,84] We suggest that both open pore structures observed

under different surface tensions can be associated with different open-pore states of the protein molecules proposed from molecular modeling.

AFM images for protein molecules adsorbed on relatively hydrophobic monolayers (surface tension below 30 mJ/m^2) showed the presence of individual MscL molecules embedded in the lipid monolayers as round nanoscale bumps (Fig. 43A). The overall vertical dimension of protein embedded in lipid monolayer of 4-5 nm is the highest among different surface. However, it is smaller than molecular dimensions in an unperturbed conformation (about 8 nm in closed conformation) due to the compression stress induced by the tip during direct physical contacts. [85] No clear indications of pore structure were found for MscL molecules. Therefore, we concluded that under low surface tension, MscL proteins retained their closed-pore conformation.

A very different structure was observed for MscL molecules embedded in less ordered, loosely packed SAMs with fluid-like packing of alkyl tails and higher surface tension between 30 and 60 mJ/m^2 (Fig. 43A2). A doughnut shape of adsorbed protein molecules was consistently observed for low and high concentrations of adsorbed proteins. The overall height of the protein molecules immersed in the alkyl monolayer is within 2.2-2.7 nm, indicating a significant flattening of the protein molecules. A clear large opening was consistently observed on the very top of these molecules. The apparent width of this opening, calculated as the distance between edges of the rim, reached 11-13 nm, and "apparent" internal pore diameter reached 8-9 nm. These values are larger than that expected for the molecules in the close-expanded or open states (Fig. 44) due to dilation and lateral stresses produced by the tip with a

radius of 10 nm and a contact diameter of 2 nm. Actual molecular dimensions estimated by deconvoluting tip shape are close to that expected from molecular models. It worth noting that a slight asymmetry of the rim height is detected for most of molecules, which could be attributed to overall tilted orientation of MscL molecules within planar monolayers.

For the MscL molecules embedded in the loosely packed lipid monolayer with estimated surface energy of 60-68 mJ/m^2, even larger opening was systematically observed for flattened and frequently slightly tilted protein molecules (Fig. 1c). The total height of the protein molecules was estimated to be close to 1.8-2.0 nm and the apparent opening increased to 14-18 nm, which is statistically different from the previous state (Fig. 1b). This shape of the molecule reflects even wider opening of the central pore as compared to previous structure even considering significant distortions contributed by the tip.

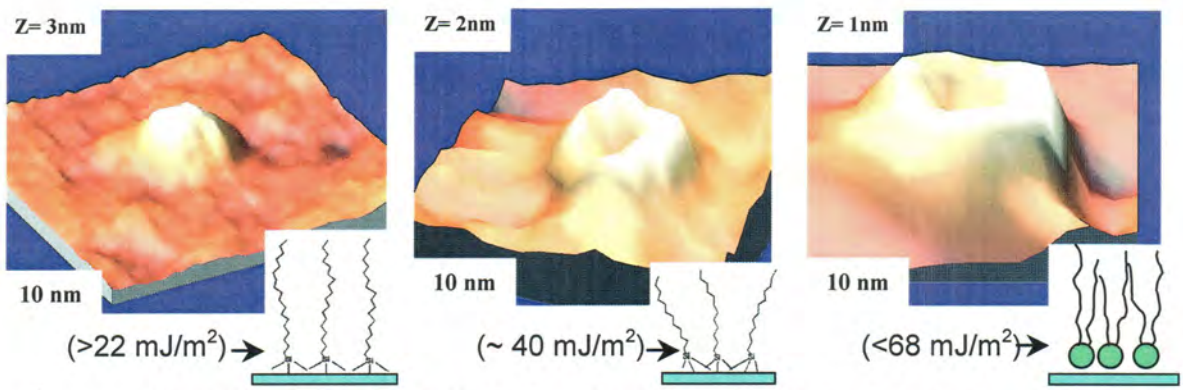

A **3D representation of MscL single molecules in different substrates**

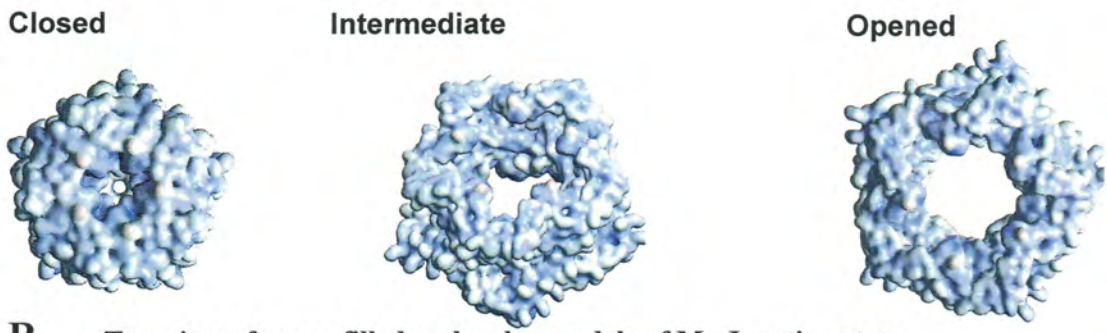

B **Top-view of space-filled molecular models of MscL gating states**

C **Side view of ribbon molecular models of MscL gating states**

Figure 43. 3D representation of MscL single molecules in different substrates in comparison with molecular models of MscL gating conformations.

The variation of geometrical dimensions of the MscL molecules in different conformational states in comparison with dimensions obtained from the AFM images are presented in Fig. 44. Both diagrams show very similar trends, which are characteristics of iris-like expansion: significant height decrease is accompanied by a correlated dramatic width increase and pore opening. "Apparent" dimensional parameters obtained directly from AFM images underestimate height and overestimate lateral dimensions as was mentioned above but the variation of the parameters still reflects a general trend expected for MscL molecules in different conformational states.

We believe that these results demonstrate that different surface tensions of organic monolayers used for immobilization of MscL molecules are instrumental in mediating protein conformation. As has been shown for protein-monolayer surface complexes, protein conformation may change dramatically depending upon the packing density of alkyl tails and the hydrophilic/hydrophobic balance of supporting organic layer. These changes are caused by both variation of the surface tension and the level of interaction/penetration of protein segments and alkyl tails. [86,87,88] Loosely packed organic monolayers provide stronger anchoring because of these reasons and possess higher surface tension that generates higher local surface forces acting on very compliant protein molecules. We suggest that this situation is similar to one developed in stressed cell membranes that results in conformation reorganizations of MscL molecules detected by direct observation and associated with two-stage the iris-like expansion suggested earlier.[89]

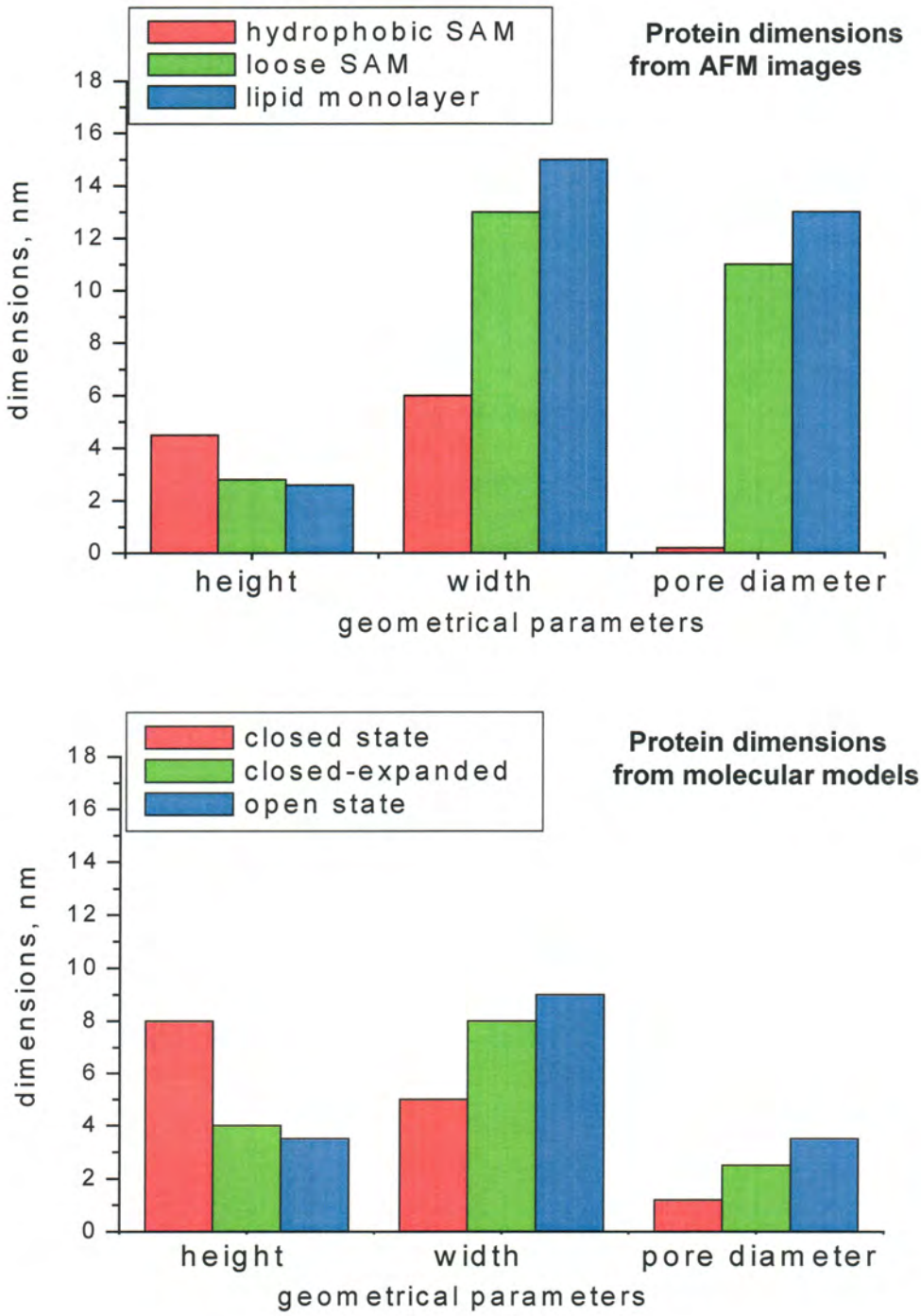

Figure 9. Geometrical parameters of MscL molecules in three different states as deduced from molecular models (top) and calculated directly from AFM images (bottom).

CHAPTER 6. GENERAL CONCLUSIONS

In the present work, we focused on understanding design principles of polymer matrix suitable for reconstitution of ion channel proteins on silicon substrates. In order to evaluate the influence of the substrate surface characteristics on conformation of ion channel proteins upon immobilization, we applied two independent approaches. As a first approach, we investigated the adsorption of Hemolysin and MscL proteins onto single crystal silicon substrate. As a second approach, the adsorption of MscL onto ODTMS SAMs surface with controlled surface energy was studied. AFM images of individual protein molecules were used for analysis of protein conformation changes during adsorption on different substrates.

Both channel proteins studied here showed signs of denaturation on substrates with high surface energy such as silicon oxide. Hemolysin adsorbs in a compact fashion due to prevailing ionic interactions of its polar head with negatively charged silicon hydroxide surface. Quite different mechanism was observed for MscL adsorption on silicon oxide. This protein formed a layer of unfolded protein on the surface. The MscL molecule is, to large extent, a hydrophobic structure with few polar amino groups hidden inside. During adsorption, the protein was forced to expose polar groups to contact with high-energy silicon surface.

The experiments on the reconstitution of the proteins into the lipid LB monolayer were intended to control the conformational state of the proteins at interfaces. In fact, the dimensions of the protein molecules within the lipid LB monolayer indicated that this system

allowed alleviate the extent of denaturation for both proteins. Hemolysin appears to keep more compact conformation than observed on the silicon surface. Effect that is more significant was observed for MscL protein. In LB layer, the protein was adsorbed in a compact fashion, without unfolding. Both, hemolysin and MscL, appear in collapsed conformation because of significant interaction with the substrate.

As an alternative approach, the MscL was reconstituted in "buffer organic layer", alkylsilane SAMs. Fabrication and characterization of a series of alkyl terminated SAMs with controlled density and surface roughness was performed in this work. The variation of densities of the SAMs enabled the analysis of the effects of surface energy on the conformation of MscL. MscL channel structures were clearly detected after protein adsorption onto low density SAM. Adsorption of MscL onto densely packed SAMs resulted in closed-pore conformation. At the same time, the quantity of adsorbed molecules on this SAM was much lower comparing to the low-density SAM. On the other hand, no protein adsorption was observed for highly hydrophobic SAM. It was concluded that the adsorbed amount and molecular organization of the MscL were controlled by surface energy of the organic SAM.

As the final step, liposome fusion technique was utilized for the reconstitution of MscL onto patterned silicon surface. A special design of the surface pattern, provided alternating areas of hydrophilic silicon surface and highly hydrophobic SAM surface. As was shown, MscL did not adsorb onto the hydrophobic surface. The developed surface pattern assured directed co-adsorption of protein embedded in liposomes predominantly on the hydrophilic

silicon areas due to liposome fusion process. AFM imaging of the patterned SAM after reconstitution of MscL, revealed localized insertion of the MscL in the areas covered with lipid monolayer. Under these conditions, MscL molecules appear as open channel structures.

Analysis of molecular dimensions of the MscL protein molecules on different substrates demonstrated that the molecular conformation of SAM-supported ion channel could be controlled by the variation of surface energy. These data were shown to be in good agreement with molecular modeling of MscL gating mechanism. The molecular structure of the MscL in lipid SAM was suggested to be the open-pore conformation of the ion channel protein. It seems that reconstitution of MscL into loosely packed SAM most probably resulted in so-called expanded conformation of the MscL, characterized with intermediate pore.

REFERENCES CITED

[1] Madou, M., "Fundamentals of Microfabrication," CRC press, 1997, pp. 500.

[2] Grace, M.S.; Church, D.R.; Kelly, C. T.; Lynn, W.F.; Cooper, T.M., *Biosensors and Bioelectronics*, **1999**, 14, 53.

[3]Fuchigami, N.; Hazel, J.; Gorbunov, V.V.; Stone, M.; Grace, M.; Tsukruk, V.V., *Biomacromolecules,* **2001**, 2, 757.

[4] Sowards, L. A.; Halsey, L. L.; Nolan, A. M.; Stone, M. O; Abstract, 217th ACS National Meeting, Anaheim, 1999.

[5] Meijer, G.C., Thermal Sensors, Bristol, UK; Philadelphia: Institute of Physics Pub., 1994.

[6] Golay, M. J. E., *The Review of Scientific Instruments.* **1947,** 18, 357.

[7] Chevrier, J-B.; Baer, K.; Slater, T., *J. Micromech. Microeng.*, **1995**, 5, 193.

[8] Yamashita, K.; Murata, A.; Okuyama, M., *Sensors& Actuators A*, **1998**, 66, 29.

[9] Kenny, T.W.; Kaiser, W.J.; Reynolds, J.K.; Rodosek, J.A., Rockstad, H.K.; Vote, E.C.; Waltman, S.B., J. *Vac. Sci. Technol.*, **1993**, 11, 797.

[10] Chang, Chung Cheng; Lieu, Chi Tsai; Hsich, Mei Kuan. *International Journal of Electronics.* **1997**, 82, 295.

[11] Gracia, I.; Santander, J.; Cane, C.; Horrillo, M. C.; Sayago, I.; Gutierrez, J. *Sensors and Actuators, B: Chemical* **2001**, B77, 409.

[12] Terashima S.; Goris R.C., Eds., *Infrared Receptors and the Trigeminal Sensory System*, Harwood Acad. Publ., Amsterdam, **1998.**

[13] Amemiya, F.; Goris, R.C.; Masuda, Y.; Kishida, R.; Atobe, Y.; Ishii, N.; Kusunoki, T., *Biomed. Res.*, **1996**, 16, 411.

[14] Campbell, A.L.; Bunning, T.; Stone, M.O.; Church, D.; Grace, M., *J. Struct. Biol.* **1999**, 126, 105.

[15] Bullock, T. H.; Diecke, P., *J. Physiology*, **1956**, 134, 47.

[16] Vondran, T.; Apel, K.-H.; Schmitz, H., *Tissue Cell*, **1995**, 27, 645.

[17] Schmitz; H.; Bleckmann, H.; Murtz, M., *Nature,* **1997**, 386, 773.

[18] Campbell A. L., Naik R. R, Sowards L.; Stone M. O. *Micron,* **2002**, 33, 211.

[19] Schmitz, H.; Bleckmann, H., *J. Comp. Physiol,* **1998**, 182, 647.

[20] Tominaga, M.; Caterina, M.J.; Malmberg, A.B.; Rosen, T.A.; Gilbert, H.; Skinner, K.; Raumann, B.E.; Basbaum, A.I.; Julius, D., *Neuron*, **1998**, 21, 531.

[21] Jones, S. E.; Naik, R. R.; Stone, M.O., *Biochenical and Biophysical Research Communications*, **2000**, 279, 208.

[22] Moe, P. C.; Levin, G.; Blount, P., *J. Biol. Chem.*, **2000**, 275(40), 31121.

[23] Blount, P.; Sukharev, S. I.; Moe, P. C.; Nagle, S. K.; Kung, C., *Biol. Cell,* **1996**, 87, 1.

[24] Blount, P; Sukharev, S. I.; Moe, P. C.; Schroeder, M. J.; Guy, H. R.; Kung, C. *EMBO J.,* **1996**, 15, 4798.

[25] Moe, P. C.; Blount, P.; Kung, C. *Mol. Microbiol.*, **1998**, 28, 583.

[26] Blount, P.; Sukharev, S. I.; Moe, P. C.; Martinac, B.; Kung, C.. *Methods Enzymol.,* **1999**, 294, 458.

[27] Moe P.C., Levin G., Blount P.,. *Biol. Chem.*, **2000,** 275, 31121.

[28] Chang G., Spencer R. H., Lee A. T., Barclay M. T, Rees D. C. *Science*, **1998**, 282, 2220.

[29] Biggin, P.C, Sansom, M.S.P., *Current Biology,* **2001**, 11, R364.

[30] Song, L.; Hobaugh, M.; Shustak, C.; Cheley, S.; Bayley, H.; Gouaux. J. E., *Science*, **1996**, 274, 1859.

[31] Tobkes, N.; Wallace, B.A.; Bayley, H., *Biochemistry*, **1985**, 24, 1915.

[32] Braha, O.; Walker, B.; Cheley, S.; Kasianowicz, J.J.; Song, L.; Gouaux, J.E.; Bayley, H., *Chemistry and biology*, **1997**, 4, 497.

[33] Kasianowicz, J.J.; Burden, D.L.; Han, L.C.; Cheley, S.; Bayley, H., *Biophysical Journa*l, **1999** 76(2), 837.

[34] Gu, L.Q.; Braha, O.; Conlan, S.; Cheley, S.; Bayley, H., *Nature*, **1999**, 398, 686.

[35] Vecsey-Smjen, B.; Knapp, S.; Mollby, R.; van der Goot, F.G., *Biochemistry,* **1999**, 38, 4296.

[36] Blount P; Moe PC. *Trends Microbiol* **1999**, 7, 420.

[37] Moe PC.; Levin G; Blount, P. *J Biol Chem* **2000**, 275, 31121.

[38] Andersen, O. S.; Nielsen, C.; Maer, A. M.; Lundbaek, J. A.; Goulian, M.; Koeppe, R. E., II. *Methods Enzymol.,* **1999**, 294, 208.

[39] Perozo, E.; Kloda A; Cortes D M; Martinac B., *J. Gen. Physiol.*, **2001**, 118, 193.

[40] Perozo, E.; Kloda A; Cortes D M; Martinac B., *Nature Struct. Biol.* **2002,** 9, 696.

[41] Cheng, Y.; Ogier, S. D.; Bushby, R. J.; Evans, S. D., *Reviews in Molecular Biotechnology* **2000**, 74, 159-174.

[42] Gopel, W.; Hesse, J.; Zemel, J.N, Eds. Sensors: A Comprehensive Study. VCH: New York, **1991.**

[43] Schillers, H.; Danker, T.; Madeja, M.; Oberleithner, H.. *J. Membr. Biol.* **2001**, 180, 205.

[44] Wise, K. D. in: Nanofabrication and Biosystems: Integrating Materials Science, Engineering and Biology, eds. Hoch, H. C.; Jelinski, L. W.; Craighead, H. G., Cambridge University Press, Cambridge, UK, 1996.

[45] Ulman, A. *Introduction to Ultrathin Organic Films*, Acad. Press, San Diego, **1991**.

[46] Jagow von G., Schägger H. A. Practical guide to membrane protein purification. San Diego: Academic Press, **1994.**

[47] Wise, K. D. in: *Nanofabrication and Biosystems: Integrating Materials Science, Engineering and Biology*, eds. Hoch, H. C.; Jelinski, L. W.; Craighead, H. G., Cambridge University Press, Cambridge, UK, 1996.

[48] Weetall, H.H., *Advances in Molecular and Cell Biology*, **1996**, 15A, 161.

[49] Song, L.; Hobaugh, M. R.; Shustak, C.; Cheley, S.; Bayley, H; Gouaux, J. E. *Science*, **1996**, 274, 1859.

[50] Jones S. E., Naik R. R., Stone M. O. *Biochemical and Biophysical Research Communications,* **2000**, 279, 208.

[51] Tsukruk, V.V.; Bliznyuk, V.N., *Langmuir*, **1998**, 14, 446.

[52] Duchet, J.; Chabert, B.; Chapel, J. P.; Gerard, J. F.; Chovelon, J. M.; Jaffrezic-Renault, N. *Langmuir*, **1997**, 13, 2271.

[53] Horr, T.J.; Ralston, J.; Smart, R. St. C., *Colloids Surf., A*; **1995**, 97, 183.

[54] Bierbaum, K.; Grunze, M.; Baski, A. A.; Chi, L. F.; Schrepp, W.; Fuchs, H., *Langmuir*, **1995**, 11, 2143.

[55] Glazier, S. A.; Vanderah, D. J.; Plant, A. L.; Bayley, H.; Valincius, G.; Kasianowicz, J. J. *Langmuir*, **2000**, 16, 10428.

[56] Glazier, S. A.; Vanderah, D. J.; Plant, A. L.; Bayley, H.; Valincius, G.; Kasianowicz, J. J., *Langmuir*, **2000**, 16, 10428.

[57] Hansma P.K., Ellings V.B., Bracker M. O., Science, **1988,** 244, 209.

[58] Morris, V.J., Kirby, A.R., Gunning A.P. Atomic force microscopy for biologists .London : Imperial College Press, 1999.

[59] Hazel, J. L.; Tsukruk, V. V., *Polym. Prepr.*, **1996**, 37, 567.

[60] Tsukruk, V.V., *Rubber Chem. Techn.*, **1997**, 70, 430.

[61] Tsukruk, V.V.; Reneker, D.H., *Polymer*, **1995**, 36, 1791.

[62] Azzam R. M. A.; Bashara N. M. Ellipsometry and polarized light, Elsevier, 1977, 529p.

[63] Neumann A.W., Spelt J. K. Applied surface thermodynamics. New York: Marcel Dekker, 1996.

[64] Berman, H.M.; Westbrook, J.; Feng, Z.; Gilliland, G.; Bhat, T.N.; Weissig, H.; Shindyalov, I.N.; Bourne, P.E., *Nucleic Acids Research*, **2000**, 28, 235.

[65] Magonov, S. N. Surface analysis with STM and AFM: experimental and theoretical aspects of image analysis, Weinheim ; New York : VCH, 1996

[66] Norde W., *Adv. Colloid Interface Sci.*, **1986**, 25, 267.

[67] Prausnitz J. M. *Journal of Chemical Thermodynamics*, **2003**, 35, 21.

[68] Czeslik, C.; Jackler, G.; Royer, C. *Spectroscopy,* **2002**, 16, 139.

[69] Walker B; Krishnasastry M; Zorn L; Kasianowicz J; Bayley H. *Journal of Biol Chem.* **1992**, 267, 109029.

[70] .Clayton J. Abstract, 222nd ACS National Meeting, Chicago, 2001.

[71] Dubois, L. H.; Zegarski, B. R. *Journal of Physical Chemistry.* **1993**, 97, 1665.

[72] Bluemel, J. *Journal of the American Chemical Society.* **1995**, 117, 2112.

[73] Ulman, A., *Chemical Reviews*, **1996**, 96, 1533.

[74] McGovern, M.E.; Kallury, K.M.R.; Thompson, M. *Langmuir*, **1994**, 10, 3607

[75] Wasserman, S.R.; Tao, Y.-T.; Whitesies, G.M. *Langmuir*, **1989**, 5, 1074.

[76] Richter, A. G.; Yu, C.-J.; Datta, A.; Kmetko, J.; Dutta, P. *Physical Review E.* **2000**, 61, 607.

[77] Almanza-Workman, A. M.; Raghavan, S.; Petrovic, S.; Gogoi, B.; Deymier, P.; Monk, D.J.; Roop, R. *Thin Solid Films,* **2003**, 423, 77.

[78] Motesharei, K.; Ghadiri, M. R. *Journal of the American Chemical Society.* **1997**, 119, 11306

[79] Cornell, B. A. *Optical Biosensors.* **2002**, 457.

[80] Dufrene Y F; Lee G. U. *Biochimica et biophysica acta.* **2000**, 1509, 14.

[81] Jass J; Tjarnhage T; Puu G. *Biophysical journal* .**2000**, 79, 3153.

[82] Fang Y; Cheley S; Bayley H; Yang *J. Biochemistry*.**1997**, 36, 9518.

[83] Adamson, A. W. Physical Chemistry of Surfaces, Wiley, 1990.

[84] Gullingsrud, J., Kostzin, D., Schulten, K., *Biophys. J.*, **2001**, 80, 2074.

[85] Magonov, S., Whangbo, M.-H. Surface Analysis with STM and SPM, VCH, Weinheim, 1996.

[86] Tan, J. L., Tien, J., Chen, C. S., *Langmuir,* **2002**, 18, 519.

[87] Sheller, N. B., Petrash, S., Foster, M. D., Tsukruk, V. V. , *Langmuir,* **1998**, 14, 4535.

[88] Petrash, S., Cregger, T., Zhao, B., Pokidysheva, E., Foster, M. D., Brittain, W., Sevastianov, V., Majkrzak, C. F. *Langmuir,* **2001**, 17, 7645.

[89] Sukharev, S. *FASEB J.*, **1999**, 13, 55.

BIOGRAPHICAL SKETCH

Maryna Ornatska was born January 19, 1974 in Kiev, Ukraine. She attended National Technological University of Ukraine «Kiev Polytechnic Institute», between September 1991 and May 1998. She received the Bachelor of Science in Chemical Engineering in 1996 and Master of Science in Biotechnology Engineering in 1998. In January 2001 she entered graduate program in the Materials Science and Engineering Department at Iowa State University. She worked as a Graduate Research Assistant at Iowa State University.

PROFESSIONAL PUBLICATIONS AND PRESENTATIONS

Peer Reviewed Articles

1. Tsukruk, V. V.; **Ornatska, M.;** Sidorenko, A; "Synthetic and bio-hybrid nanoscale biomacromolecular layers with tailored surface functionalities" , *Progr. Organic Coatings*, accepted
2. **Ornatska, M.;** Jones, S. E.; Naik, R. R.; Stone, M.; Tsukruk, V. V.; "Conformational transitions of mechanosensitive channel proteins induced by variable surface tension" *Biomacromolecules,* submitted
3. Peleshanko, S.; Sidorenko, A.; Larson, K.; Villavicencio, O.; **Ornatska, M.**; McGrath, D. V.; Tsukruk, V. V. "Langmuir-Blodgett monolayers from lower generation amphiphilic monodendrons" *Thin Solid Films* **2002**, 406, 233-240.

Preprints and Abstracts

1. Tsukruk, V.V.; **Ornatska, M.**; "Mechanosensitive proteins on silicon with controlled surface energy" Air Force Office for Scientific Research program review, Duck Key, FL, February, 2003
2. Tsukruk, V.V.; **Ornatska, M.**; Sidorenko A.; "Biomacromolecular coatings immobilized on microelectronic-related surfaces", Key Stone, CL, 2002
3. Tsukruk, V.; **Ornatska, M.**; Markutsya, S.; Peleshanko, S. "Robust and elastic films from multilayered polymer-nanoparticle composites" Abstracts of Papers, 224th ACS National Meeting, Boston, MA, 2002

Professional presentations

1. February 2002 Oral Presentation "Biomacromolecular coatings immobilized on microelectronic-related surfaces", Air Force Office for Scientific Research program review, Key Stone, CL.
2. August 2002 Poster presentation "Robust and elastic films from multilayered polymer-nanoparticle composites", 224th ACS National Meeting, Boston, MA.
3. February 2003 Oral Presentation "Mechanosensitive proteins on silicon with controlled surface energy" Air Force Office for Scientific Research program review, Duck Key, FL